nature cell biology

An extracellular-matrix-specific GEF–GAP interaction regulates Rho GTPase crosstalk for 3D collagen migration

Matthew L. Kutys[1,2] and Kenneth M. Yamada[1,2]

Rho-family GTPases govern distinct types of cell migration on different extracellular matrix proteins in tissue culture or three-dimensional (3D) matrices[1–3]. We searched for mechanisms selectively regulating 3D cell migration in different matrix environments[4,5] and discovered a form of Cdc42–RhoA crosstalk governing cell migration through a specific pair of GTPase activator and inhibitor molecules. We first identified βPix, a guanine nucleotide exchange factor (GEF), as a specific regulator of migration in 3D collagen using an affinity-precipitation-based GEF screen. Knockdown of βPix specifically blocks cell migration in fibrillar collagen microenvironments, leading to hyperactive cellular protrusion accompanied by increased collagen matrix contraction. Live FRET imaging and RNAi knockdown linked this βPix knockdown phenotype to loss of polarized Cdc42 but not Rac1 activity, accompanied by enhanced, de-localized RhoA activity. Mechanistically, collagen phospho-regulates βPix, leading to its association with srGAP1, a GTPase-activating protein (GAP), needed to suppress RhoA activity. Our results reveal a matrix-specific pathway controlling migration involving a GEF–GAP interaction of βPix with srGAP1 that is critical for maintaining suppressive crosstalk between Cdc42 and RhoA during 3D collagen migration.

Distinct biological responses of cells to interactions with different extracellular matrix (ECM) proteins are necessary for efficient tissue development and wound repair, and are often deregulated in cancer[6–9]. Integrin binding to ECM proteins triggers selective activation of Rho GTPases, which induce cell polarization, cytoskeletal rearrangements, and contractile responses required for efficient migration in different microenvironments[10–12]. However, a fundamental unanswered question is how specific Rho GTPase signalling pathways governing migration are regulated differentially by specific ECM proteins. These GTPases are regulated by GEFs, which activate them by facilitating the exchange of GDP for GTP (ref. 13). We reasoned that adhesion to specific ECM molecules, such as collagen and fibronectin, would trigger differential GEF activation to regulate cell migratory responses.

Nucleotide-free, dominant-negative Rho GTPase mutants can be used for affinity-isolation of activated GEFs (refs 14,15). We initially focused on GEFs for Rac1 because of its well-established role in driving 2D and 3D motility through coordination of lamellipodial dynamics[16]. In an ECM-based screen, we identified active GEFs binding to recombinant RacG15A, a Rac1 nucleotide-free mutant, from lysates of primary human foreskin fibroblasts (HFFs) undergoing steady-state migration in collagen, fibronectin or ECM-free environments. We used an unbiased screening approach[14,15] for identification of active GEFs in cells migrating in specific ECM environments by identifying protein bands in Coomassie-stained polyacrylamide gels that bound selectively to RacG15A in different ECM environments (Supplementary Fig. 1a). Multiple GEFs were isolated that showed increased activity on both fibronectin and collagen (Fig. 1a and Supplementary Fig. 1b), but the Rac1/Cdc42 GEF βPix was activated robustly and specifically only during migration on collagen (Fig. 1b). βPix exists at multiple subcellular sites, including focal adhesions and plasma membrane, consistent with differential functions[17–19]. We therefore tested for altered localization of βPix during fibroblast migration on fibronectin versus fibrillar collagen. As expected, both immunofluorescence staining for endogenous βPix and live-cell imaging of GFP–βPix showed strong localization to focal adhesions during migration on fibronectin and 3D cell-derived matrices (CDMs), where the primary ECM ligand is fibronectin[20] (Fig. 1c and Supplementary Fig. 1d–g). Surprisingly, we found a pronounced decrease in both endogenous and GFP–βPix focal

[1]Laboratory of Cell and Developmental Biology, National Institute of Dental and Craniofacial Research, National Institutes of Health, Bethesda, Maryland 20892-4370, USA.
[2]Correspondence should be addressed to M.L.K. or K.M.Y. (e-mail: kutysml@mail.nih.gov or kyamada@mail.nih.gov)

Received 14 February 2014; accepted 10 July 2014; published online 24 August 2014; DOI: 10.1038/ncb3026

adhesion localization in fibroblasts migrating on both fibrillar collagen and 3D collagen (Fig. 1c and Supplementary Fig. 1d–g). Subcellular fractionation revealed that on fibrillar collagen, endogenous βPix transitioned from detergent-soluble to -insoluble fractions (Fig. 1d), and live-cell GFP–βPix imaging showed a patchwork localization on ventral cell membranes in amorphous, persistent aggregates of variable size that polarized to leading-edge protrusions, but did not co-localize with paxillin (Supplementary Fig. 1g). These data demonstrate that the intracellular location of βPix changes markedly when cells migrate on collagen compared with fibronectin, supporting the existence of ECM-specific functions observed in the initial GEF screen.

We next tested whether βPix has collagen-specific functions in cell morphology or migration. Lentiviral-mediated knockdown of βPix in HFFs with two independent short hairpin RNAs (shRNAs; Supplementary Fig. 1c) revealed that loss of βPix resulted in cells with rounded morphology, inability to spread in 3D collagen matrices, and severe motility defects in 3D collagen; in contrast, there were no effects in CDM (Fig. 1e,f,i and Supplementary Video 1). This phenotype was characterized by rapid, transient formation of spatially deregulated cell protrusions (Fig. 1f arrowheads, Fig. 1j) with minimal cell motility compared with nonspecific shRNA control cells in 3D collagen (Fig. 1g,k). In addition to three fibroblast lines (HFF, BR5, BJ5ta), this collagen-specific βPix knockdown phenotype was observed in additional cell types including primary human osteoblasts, aortic smooth muscle cells, umbilical vein endothelial cells, and invasive epithelial-derived adenocarcinoma cells (Supplementary Fig. 1h–j). Loss of βPix led to severe morphological and migratory defects specific to collagen environments in all cell types we tested (Supplementary Fig. 1k,l). Although no obvious alterations were observed in focal adhesions, actin cytoskeleton or microtubules (Supplementary Fig. 2a), the collagen fibres adjacent to βPix knockdown cells were remodelled robustly by contraction/compaction that often tore holes in the collagen matrix (Fig. 1h, asterisks). Interestingly, even high concentrations of globular collagen could not fully recapitulate the characteristic βPix knockdown phenotype in 3D collagen or on thin, fibrillar collagen substrates (Supplementary Video 2 and Fig. 1k). These fibrillar collagen substrates are thin for improved optical imaging, but they retain the fibrillar structure of 3D collagen gels and underscore the importance of using more-physiological polymerized collagen fibres rather than globular monomeric collagen. Expression of shRNA-resistant GFP–βPix at near-endogenous levels in cells with knockdown of endogenous βPix rescued both morphological and migratory defects (Supplementary Figs 2b,c and 4d). Thus, βPix has a critical, matrix-specific role in cell migration in fibrillar collagen environments, with knockdown leading to hyper-protrusive, hyper-contractile cells incapable of efficient migration.

As βPix is a dual-specificity GEF (ref. 21), we tested its effects on Rac1 and Cdc42 activity during migration in fibrillar collagen microenvironments. βPix bound specifically to the nucleotide-free mutant of Rac1, with no binding to a recombinant wild-type or a constitutively active mutant (Supplementary Fig. 2j). Consistent with its reported function as a Rac1/Cdc42 GEF (ref. 21), βPix knockdown resulted in collagen-specific decreases in both Rac1 (∼20%) and Cdc42 (∼30%) activities (Fig. 2a,b). As was found for RacG15A, βPix differentially bound to recombinant Cdc42G15A (Fig. 2c). It exhibited increased but partial co-localization with Cdc42 in leading edge protrusions (Supplementary Fig. 3a) during migration on fibrillar collagen, but not fibronectin. Independent knockdowns using a single short interfering RNA (siRNA) for each protein were performed to determine whether depletion of Rac1 or Cdc42 would recapitulate the βPix knockdown phenotype in 3D collagen (Fig. 2d and Supplementary Fig. 2d–i). Surprisingly, we found that knockdown of Cdc42, but not Rac1, fully mimicked βPix knockdown in 3D collagen. Rac1 knockdown cells mirrored nonspecific siRNA controls, whereas Cdc42 knockdowns exhibited the rounded, hyper-contractile morphology observed with loss of βPix (Fig. 2e,f,h). We used multiple Rac-isoform knockdowns to rule out compensatory roles of other Rac isoforms (Rac2, Rac3) after Rac1 knockdown (Supplementary Fig. 2d–i), indicating that the collagen-βPix knockdown phenotype was due to loss of Cdc42 activity, but not Rac1. This deregulated protrusive behaviour of Cdc42- or βPix-depleted cells was accompanied by defective migration in both 3D and thin fibrillar collagen environments (Supplementary Video 3 and Fig. 2i), along with physical tearing of holes in the surrounding matrix. These findings are consistent with a report that loss of Cdc42 in 3D microenvironments leads to temporally and spatially deregulated protrusions and impaired leading edge coordination[22]. We therefore investigated whether βPix regulates the localization and activity of Cdc42 under different ECM conditions. Imaging a single-chain Cdc42 biosensor based on intramolecular fluorescence resonance energy transfer[23] (FRET) revealed that on fibronectin, Cdc42 activity remains polarized towards the leading edge of migrating cells expressing either nonspecific or βPix shRNA (Fig. 2g). On collagen, Cdc42 activity was also polarized to the leading edge in the same regions where βPix was found to uniquely localize on the membrane. In contrast, βPix knockdown on fibrillar collagen led to a loss of this polarization and decreased overall Cdc42 activity (Fig. 2g and Supplementary Fig. 2l,m). In addition, we observed similar collagen-specific decreases in Cdc42 FRET and loss of FRET polarization in 3D collagen, but not a 3D cell-derived matrix (Supplementary Fig. 2k), further establishing that βPix acts through Cdc42, but not Rac1, to coordinate migration in fibrillar collagen environments.

As a result of the strong collagen contraction phenotype associated with loss of βPix, we speculated that βPix/Cdc42 knockdown might increase RhoA activity during migration in fibrillar collagen environments. We assayed intracellular RhoA activity during fibronectin or fibrillar collagen migration in the presence and absence of βPix. Knockdown of βPix resulted in 40–60% increased intracellular RhoA activity in fibrillar collagen, but not fibronectin (Fig. 3a,b), with similar increases during 3D collagen migration (Supplementary Fig. 3e). Importantly, knockdown of Cdc42, but not Rac1, also increased intracellular RhoA activity levels on fibrillar collagen (Fig. 3c,d). We next used a single-chain RhoA FRET biosensor[23,24] to determine RhoA activity and localization during live-cell migration. Cells migrating on fibronectin exhibited a gradient of RhoA activity that was highest at the rear of the cell and decreased towards the leading edge (Fig. 3e). This localization pattern was also observed during migration on fibrillar collagen; however, after βPix knockdown, we observed a striking loss of this RhoA gradient with a general elevation of RhoA activity (Fig. 3e–g). Again, the loss of front–back RhoA FRET segregation and elevation in activity were observed in 3D collagen, but not a 3D cell-derived matrix (Supplementary

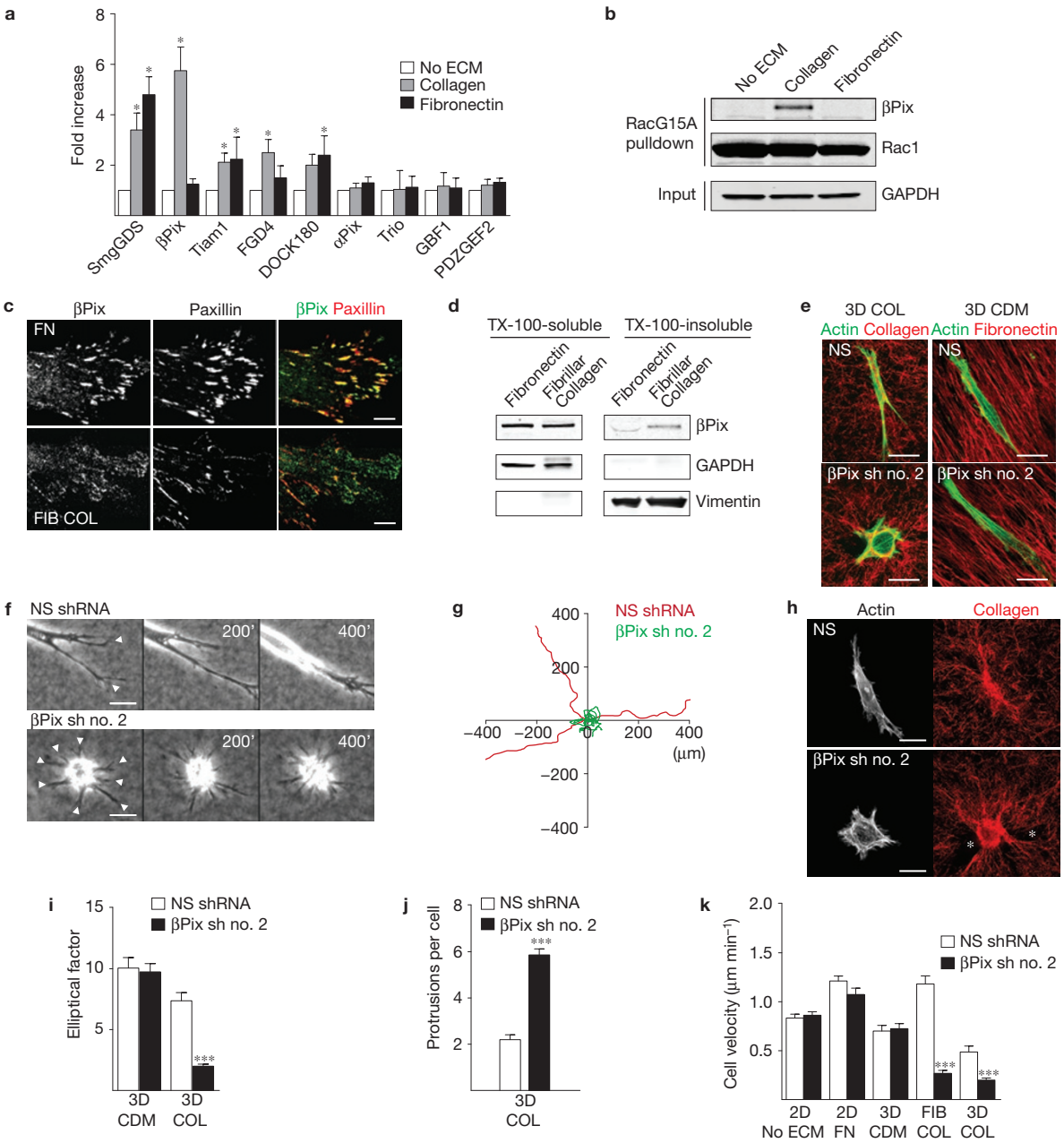

Figure 1 Loss of βPix leads to collagen-specific morphological and migratory defects. (**a**) Quantification of western blot band intensities of select GEFs isolated from the RacG15A ECM-GEF screen. Values are fold intensity increase above the No ECM condition ($n=3$ independent western blots, mean ± s.e.m., one-way ANOVA with Bonferroni multiple-comparison correction). (**b**) Western blot validation of βPix binding to RacG15A during migration on collagen. (**c**) Composite images of the leading edge of HFFs show loss of βPix localization to focal adhesions during migration on fibrillar collagen (FIB COL) but not fibronectin (FN). HFFs were immunostained for endogenous paxillin (red) and βPix (green); yellow indicates co-localization. See Supplementary Fig. 1d for the whole-cell images. Scale bars, 15 μm. (**d**) Triton X-100 fractionation of HFFs migrating on fibronectin or fibrillar collagen reveals a shift of βPix from the soluble (GAPDH) to the insoluble (vimentin) fraction during migration on collagen, observed in three independent experiments. (**e**) Morphological analysis of βPix knockdown in 3D fibrillar collagen (COL; red, reflection microscopy) versus a 3D cell-derived matrix (CDM; red, fibronectin) reveals defects in cell elongation after loss of βPix specific to 3D collagen. Scale bars, 25 μm. (**f**) Representative phase time-lapse of nonspecific (NS) and βPix shRNA fibroblasts migrating in 3D collagen. White arrowheads indicate cellular protrusions; scale bars, 25 μm. (**g**) Migratory tracks of three NS (red) and βPix (green) shRNA fibroblasts in 3D collagen reveal loss of persistent, directional motility after βPix knockdown. (**h**) Analysis of collagen fibres (red, reflection microscopy) adjacent to NS and βPix shRNA cells reveals robust collagen contraction and remodelling with βPix knockdown (physical holes, asterisks). Scale bars, 25 μm. (**i**) Quantification of cell elliptical factor (maximal length/width) in 3D collagen versus a 3D cell-derived matrix after loss of βPix. $n=44$, 46, 30 and 35 cells for NS CDM, βPix sh no. 2 CDM, NS COL and βPix sh no. 2 COL were assessed across three independent experiments (mean ± s.e.m., *t*-tests). (**j**) Quantification of cell protrusions (**e**, white arrowheads) after fixation and phalloidin staining of βPix knockdown cells in 3D collagen. $n=36$ cells for both NS and βPix shRNA were assessed across three independent experiments (mean ± s.e.m., *t*-tests). (**k**) Quantification of cell velocities after βPix knockdown in different ECM conditions. $n=20$–25 cells for NS and βPix shRNA in each matrix condition were assessed across three independent experiments (mean ± s.e.m., *t*-tests). Statistical source data can be found in Supplementary Table 2. $^{***}P<0.001$, $^{*}P<0.05$. Uncropped images of blots are shown in Supplementary Fig. 6.

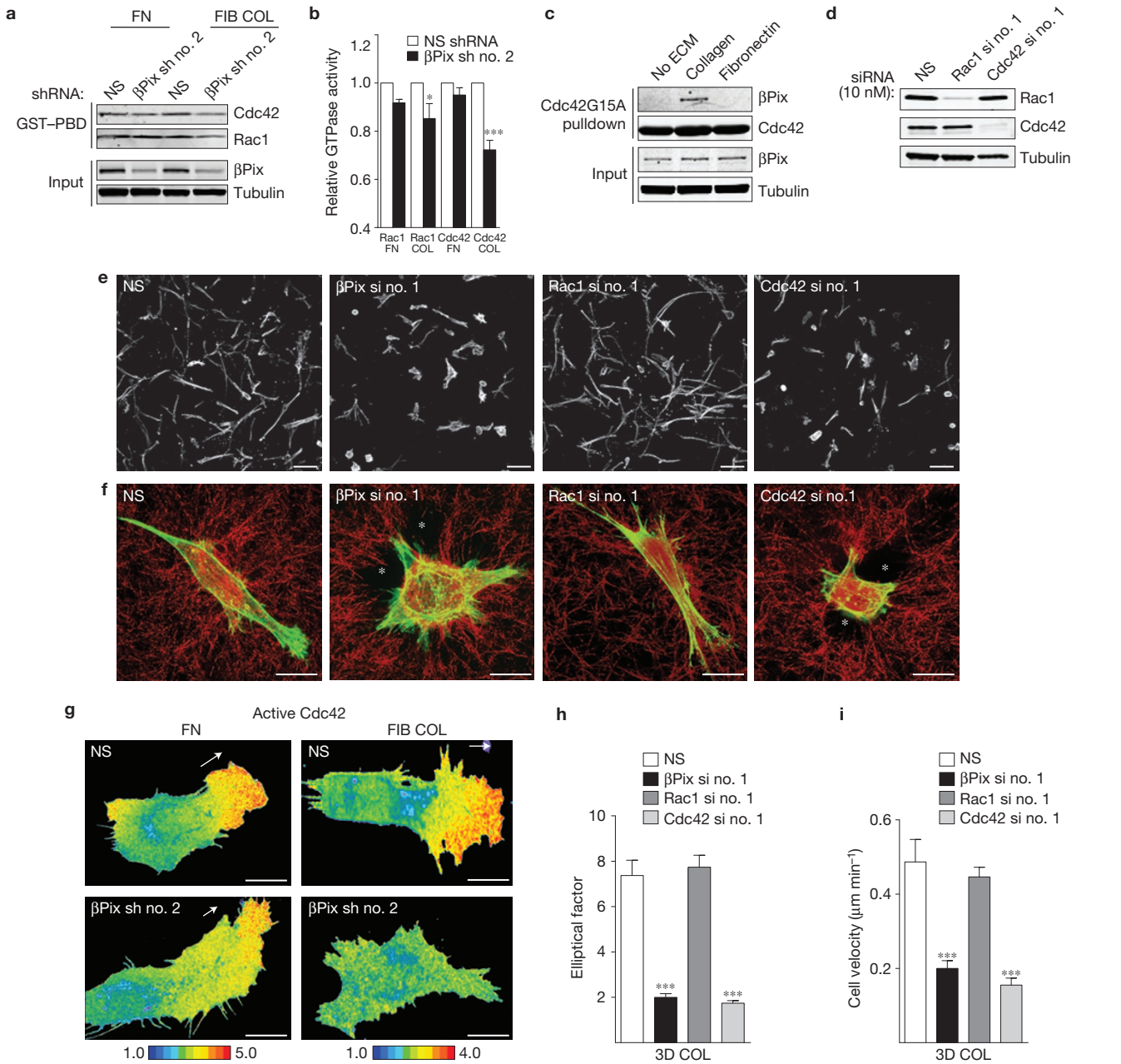

Figure 2 βPix controls the activity and localization of Cdc42 during 3D collagen migration. (**a**) Active Rac1 and Cdc42 were isolated using GST–PBD from NS and βPix shRNA-expressing HFFs migrating on fibronectin (FN) or fibrillar collagen (FIB COL). (**b**) Quantification of western blot band intensity revealed collagen-specific losses in both Rac1 (~20%) and Cdc42 (~30%) activity after depletion of βPix ($n=3$ independent western blots, mean ± s.e.m., *t*-tests). (**c**) βPix also binds specifically to recombinant Cdc42G15A in lysates from cells migrating on collagen, but not fibronectin. The result represents three independent experiments. (**d**) Single, independent siRNA treatments (10 nM) targeting Rac1 or Cdc42 were sufficient to deplete endogenous protein levels. (**e**) siRNA-treated HFFs were embedded in 3D collagen gels and incubated overnight in complete media. Cells were then fixed and stained with rhodamine–phalloidin. Maximum projections of 150 μm sections of the actin-labelled gels revealed that knockdown of Cdc42 mimicked the βPix knockdown morphology, with no defects observed with Rac1 knockdown. Scale bars, 50 μm. (**f**) Higher-power images of actin-labelled (green), siRNA-treated fibroblasts in relation to the surrounding collagen fibres (red, reflection microscopy). Knockdown of Cdc42 mimics the morphology, protrusive, and highly contractile phenotype of βPix knockdown. Holes torn in the collagen matrix are indicated by white asterisks; scale bars, 25 μm. (**g**) Maximum projections of confocal stacks of live-fibroblast migration expressing a Cdc42 biosensor on fibronectin or fibrillar collagen. Active Cdc42 is polarized towards the leading edges during migration on fibronectin in fibroblasts expressing NS or βPix shRNA. After knockdown of βPix on collagen, polarization of Cdc42 activity is lost, and overall activity is decreased. Pseudocolour intensity scales were maintained for each matrix condition; scale bars, 25 μm. White arrows designate the direction of leading edge protrusions. (**h**) Quantification of cell elliptical factor (maximal length/width) in 3D collagen after Rac1 or Cdc42 siRNA treatments. $n=35$, 30, 35 and 31 cells for NS, βPix, Rac1 and Cdc42 siRNA were assessed across three independent experiments. (**i**) Quantification of cell velocity in 3D collagen for Rac1 or Cdc42 siRNA treatments. $n=25$, 24, 22 and 24 cells for NS, βPix, Rac1 and Cdc42 siRNA were assessed across three independent experiments. For **h**,**i**, data are given as mean ± s.e.m., one-way ANOVA with Bonferroni multiple-comparison correction. Statistical source data can be found in Supplementary Table 2; $^{***}P<0.001$, $^{*}P<0.05$. Uncropped images of blots are shown in Supplementary Fig. 6.

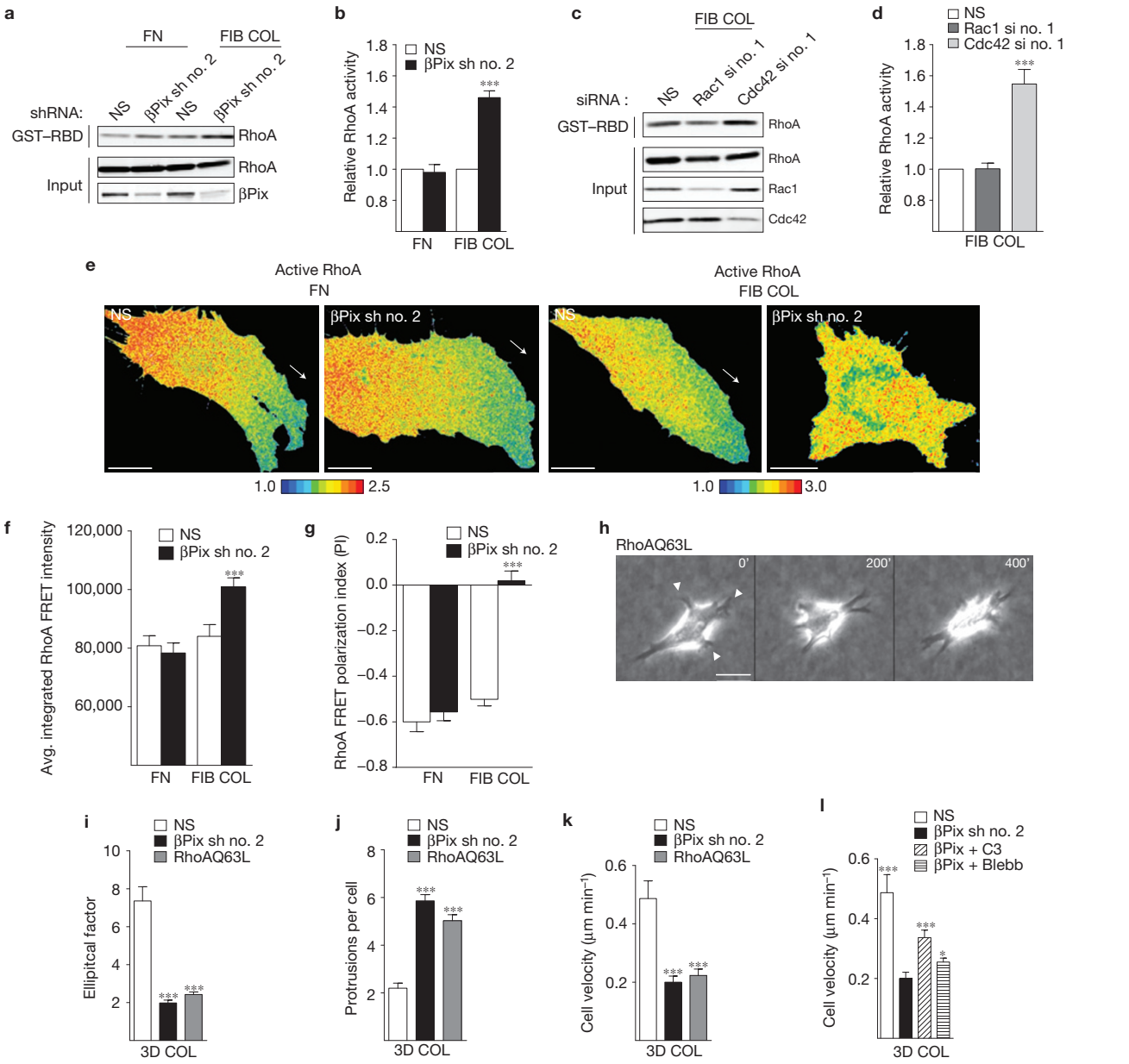

Figure 3 βPix acts through Cdc42 to suppress and localize RhoA activity during migration in 3D collagen. (**a**,**b**) RhoA activity determined using GST–RBD binding from NS and βPix shRNA-expressing HFFs migrating in fibronectin or fibrillar collagen environments; collagen-specific increases (40–60%) in RhoA activity with loss of βPix (mean ± s.e.m., $n = 3$ independent western blots, *t*-tests). (**c**,**d**) Similarly, knockdown of Cdc42, but not Rac1, during migration on fibrillar collagen leads to increased intracellular RhoA activity (mean ± s.e.m., $n = 3$ independent western blots, one-way ANOVA with Bonferroni correction). (**e**) Maximum projections of confocal stacks of live-fibroblast migration expressing a RhoA biosensor on fibronectin (FN) or fibrillar collagen (FIB COL). Knockdown of βPix on collagen results in overall elevation of RhoA activity accompanied by a loss of front–back segregation of RhoA activity. Pseudocolour intensity scales were identical for each matrix condition; scale bars, 25 μm. White arrows designate direction of leading edge protrusions. (**f**) Average integrated whole-cell RhoA FRET intensity on FN versus FIB COL. $n = 10$ cells for NS FN, βPix sh no. 2 FN, NS FIB COL and βPix sh no. 2 FIB COL were assessed across three independent experiments (mean ± s.e.m., *t*-test). (**g**) Quantification of the RhoA FRET polarization index on FN versus FIB COL. $n = 10$ cells for NS FN, βPix sh no. 2 FN, NS FIB COL and βPix sh no. 2 FIB COL were assessed across three independent experiments (mean ± s.e.m., *t*-test). (**h**) Phase-contrast time-lapse images (Supplementary Video 4) of an HFF expressing low levels of GFP–RhoAQ63L in 3D collagen reveal rounded morphology, spatially and temporally deregulated protrusions (white arrowheads) and loss of persistent migration. Scale bars, 25 μm. (**i**) Quantification of cell elliptical factor (maximal length/width) in cells expressing low levels of GFP–RhoAQ63L in 3D collagen. $n = 30$, 35 and 29 cells for NS, βPix sh no. 2 and RhoAQ63L were assessed across three independent experiments. (**j**) Quantification of cell protrusions in cells with low-level GFP–RhoAQ63L expression in 3D collagen. $n = 36$, 36 and 29 cells for NS, βPix sh no. 2 and RhoAQ63L were assessed across three independent experiments. (**k**) Quantification of cell velocity in cells with low GFP–RhoAQ63L expression in 3D collagen. $n = 25$, 24 and 21 cells for NS, βPix sh no. 2 and RhoAQ63L were assessed across three independent experiments. (**l**) βPix shRNA fibroblasts were cultured overnight in 3D collagen gels in the presence of cell-permeable C3 transferase (2 μg ml^{-1}) or blebbistatin (25 μM). $n = 25$, 24, 20 and 20 cells for NS, βPix sh no. 2, βPix + C3 and βPix + Blebb were assessed across three independent experiments. For **i**–**l**, data are given as mean ± s.e.m., one-way ANOVA with Bonferroni multiple-comparison correction Statistical source data can be found in Supplementary Table 2; $^{***}P < 0.001$, $^{*}P < 0.05$. Uncropped images of blots are shown in Supplementary Fig. 6.

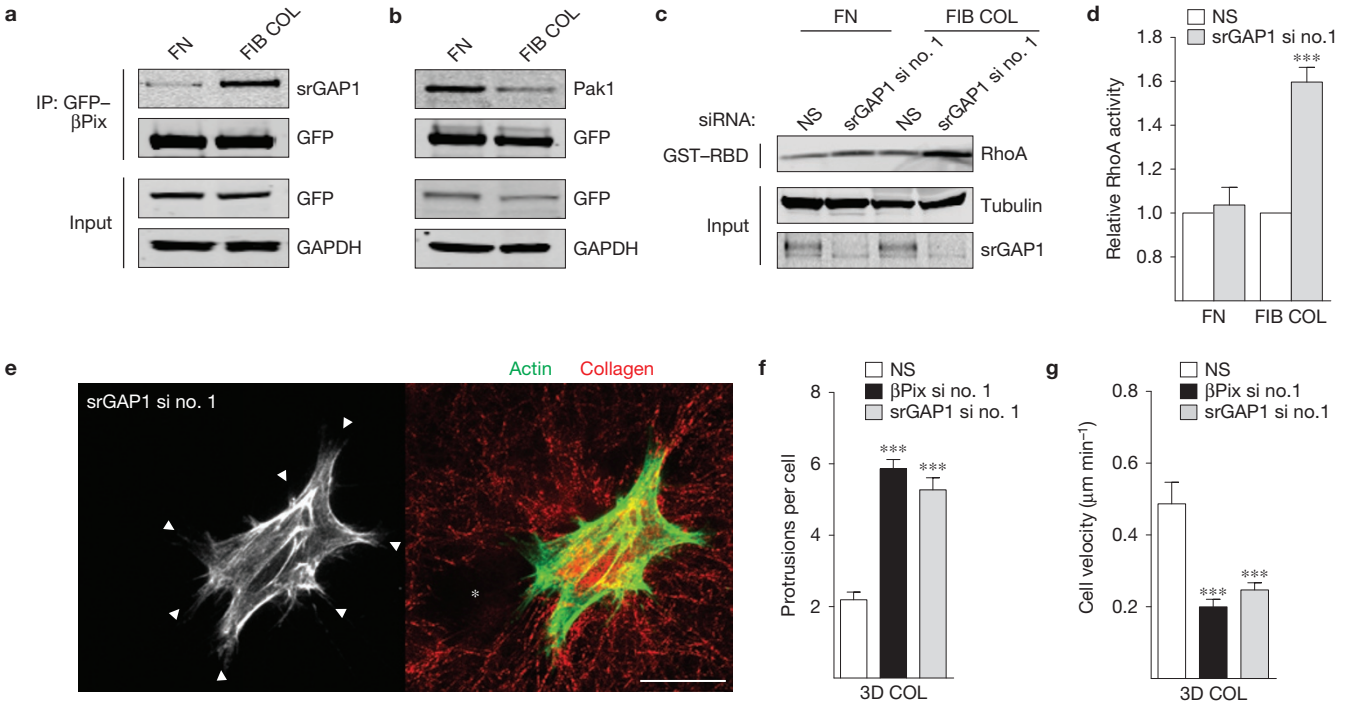

Figure 4 A collagen-specific GEF–GAP interaction between βPix and srGAP1 regulates suppression of RhoA activity. (**a**) Immunoprecipitation of GFP–βPix from βPix knockdown/rescue HFFs migrating on fibronectin (FN) versus fibrillar collagen (FIB COL) identifies a collagen-specific GEF–GAP interaction between βPix and srGAP1. (**b**) Concurrent decreased association of βPix with the known effector Pak1 when migrating on fibrillar collagen. Blots are representative of three independent experiments. (**c**) RhoA activity determined by GST–RBD binding from NS and srGAP1 siRNA-treated HFFs migrating on fibronectin or fibrillar collagen environments. (**d**) Quantification of bands again revealed a 40–60% collagen-specific increase in RhoA activity after loss of srGAP1 (mean ± s.e.m., $n = 3$ independent western blots, *t*-tests). (**e**) srGAP1 knockdown HFFs were cultured overnight in 3D collagen gels. Fixation and labelling with Alexa488–phalloidin revealed a rounded, protrusive (white arrowheads) morphology akin to βPix knockdown. Similarly, srGAP1 knockdown fibroblasts severely alter collagen fibre arrangement (red, reflection microscopy) adjacent to the cell. Hole in matrix marked by white asterisk; scale bar, 25 μm. (**f**) Quantification of cell protrusions in cells treated with srGAP1 siRNA in 3D collagen. $n = 36$, 36 and 24 cells for NS, βPix si no. 1 and srGAP1 si no. 1 were assessed across three independent experiments (mean ± s.e.m., one-way ANOVA with Bonferroni multiple-comparison correction). (**g**) Quantification of cell velocity in cells treated with srGAP1 siRNA in 3D collagen. $n = 25$, 24 and 21 cells for NS, βPix si no. 1 and srGAP1 si no. 1 were assessed across three independent experiments (mean ± s.e.m., one-way ANOVA with Bonferroni multiple-comparison correction). Statistical source data can be found in Supplementary Table 2; $^{***}P < 0.001$. Uncropped images of blots are shown in Supplementary Fig. 6.

Fig. 3b), confirming the suppressive crosstalk mechanism between βPix/Cdc42 and RhoA in collagen microenvironments. We examined whether artificial increases in RhoA activity alone could mimic βPix knockdown in 3D collagen. Low-level overexpression of constitutively active RhoAQ63L, as determined by fluorescence intensity, not only mimicked the rounded morphology (Fig. 3h,i) and robust collagen contraction (Supplementary Fig. 3c), but notably also the deregulated, hyper-protrusive behaviour (Fig. 3h,j); expressing RhoAQ63L at comparable levels in HFFs migrating in a cell-derived matrix did not perturb the morphology or lead to hyper-protrusive behaviour. Migration in fibrillar collagen environments (Supplementary Video 4 and Fig. 3k) was also significantly inhibited with low RhoAQ63L expression. Finally, to test directly whether inhibiting RhoA could partially rescue the βPix knockdown phenotype, we treated βPix knockdown cells with the RhoA inhibitor C3 transferase, or with blebbistatin to inhibit the RhoA effector myosin II. Treating βPix knockdown cells in 3D collagen with C3 transferase significantly rescued both morphology and migration and blebbistatin rescued the morphology with slight increases in motility (Fig. 3l and Supplementary Fig. 3d). We conclude that βPix acts through Cdc42 to suppress and localize RhoA activity during migration in fibrillar collagen environments.

To address mechanistically how βPix acts through Cdc42 to suppress RhoA, we used GFP–βPix knockdown/rescue fibroblasts to isolate the proteins that bound differentially to βPix from cells undergoing migration on fibronectin versus fibrillar collagen (Supplementary Figs 2b and 4a). Immunoblotting for known binding partners such as Pak1 revealed decreased association on collagen compared with fibronectin, confirming differential binding to βPix (Fig. 4b). Unexpectedly, mass spectrometry analysis of a strong band with a relative molecular mass of about 130,000 revealed a collagen-specific association between βPix and the RhoGAP srGAP1 in both HFFs (Fig. 4a) and MDA-MB-231 cells (Supplementary Fig. 4h). GAPs inactivate Rho proteins by stimulating their intrinsic GTPase activity and are critical elements in inhibitory Rho family crosstalk[4,25,26]. Depending on the context, srGAP1 can promote the GTP hydrolysis of RhoA, Cdc42 or Rac1 (ref. 27), and overexpression of srGAP1 can suppress protrusive plasma membrane dynamics[28].

To examine the role of srGAP1 in the βPix/Cdc42 collagen pathway, we performed RNAi knockdown (Supplementary Fig. 3f) and assayed

for intracellular RhoA activity. Intracellular RhoA activity levels increased significantly after loss of srGAP1 during fibrillar collagen migration but not on fibronectin (Fig. 4c,d), with no change in Rac1 activity during migration of collagen (Supplementary Fig. 3h). Knockdown of srGAP1 fully mimicked the phenotype characteristic of βPix and Cdc42 knockdown in 3D collagen (Supplementary Video 5), that is, rounded cells with hyperactive, de-localized protrusions, loss of persistent motility and increased contraction of the adjacent collagen matrix (Fig. 4e–g and Supplementary Fig. 3f,g). This result identifies an interaction between a GEF–GAP pair that mediates Cdc42 and RhoA crosstalk. This mechanism involving βPix/Cdc42/srGAP1 serves to locally suppress RhoA activity and promote efficient cell migration in fibrillar collagen environments.

Having identified a collagen-specific role for βPix, we searched for mechanisms regulating βPix in different matrix conditions. We first tested for integrin-specific regulation of βPix using certain anti-integrin monoclonal antibodies that can mimic full integrin ligation and adhesive function[29]. Using loss of focal adhesion localization as a read-out of signalling to βPix (as observed on fibrillar collagen, Fig. 1c), we assayed the localization of GFP–βPix in knockdown/rescue cells migrating on substrates coated with antibodies against β1, α5 and α2 integrin. GFP–βPix strongly co-localized to focal adhesions stained for paxillin on glass or substrates targeting β_1 and α_5 integrin (Fig. 5a). However, on substrates targeting α_2 integrin, GFP–βPix localization to focal adhesions was greatly diminished, even though paxillin-containing focal adhesions were formed normally. Conversely, treatment of cells migrating in 3D collagen with inhibitory antibodies against specific integrins confirmed specificity for the $\alpha_2\beta_1$ integrin by blocking migration (Supplementary Fig. 4b). Thus, the α_2 subunit of $\alpha_2\beta_1$ integrin is important for mediating βPix function during migration in fibrillar collagen environments.

Regulation of βPix function has been ascribed to multiple phosphorylation sites on the protein[30]. To determine whether specific phosphorylation sites were important for βPix function during collagen migration, we performed phosphoproteomics on GFP–βPix isolated from knockdown/rescue cells during migration on fibronectin versus fibrillar collagen (Supplementary Fig. 4c). We identified a selective loss of threonine phosphopeptides at Thr 526 only during fibrillar collagen migration, and confirmed by western blotting decreased threonine phosphorylation on βPix during migration on fibrillar collagen compared with fibronectin (Fig. 5b). This matrix-specific threonine phosphorylation was lost after mutating Thr 526 to alanine (T526A; Fig. 5b) in GFP–βPix knockdown/rescue HFFs, confirming that the phosphorylation of Thr 526 is altered during migration on fibronectin versus fibrillar collagen. Thr 526 phosphorylation is crucial for contextual Rac1 activation[31] and βPix translocation to focal complexes[32], consistent with our findings of loss of these actions during migration on collagen. To determine whether absence of Thr 526 phosphorylation is important for βPix function in collagen, we generated stable βPix knockdown/rescue fibroblasts with either phospho-dead (KDR-T526A) or phospho-mimetic (KDR-T526E) mutations, with the hypothesis that mimicking phosphorylation at Thr 526 would prevent morphological and migratory rescue. As predicted, re-expression of βPix with a phospho-mimetic mutation at Thr 526 could not rescue the spreading and collagen contraction/remodelling defects of βPix knockdown (Fig. 5c and Supplementary Fig. 4d), whereas T526A βPix-expressing cells were fully rescued morphologically. In addition, T526E cells could not rescue cell migration in 3D collagen gels, but T526A expression mirrored migratory velocities of rescued KDR-WT cells (Fig. 5d). Similar morphological and migratory phenotypes were observed for βPix knockdown/rescue phosphovariants in MDA-MB-231 adenocarcinoma cells in 3D collagen (Supplementary Fig. 4e–g). Mechanistically, immunoprecipitation of GFP–βPix knockdown/rescue phosphovariants during migration on fibrillar collagen revealed that the βPix phosphorylation mimetic (T526E) had decreased association with srGAP1, but not Cdc42 (Fig. 5e). These data indicate that loss of phosphorylation at Thr 526 on βPix is essential for its association with srGAP1 during fibrillar collagen migration.

To investigate the upstream regulation of Thr 526 on βPix during migration in fibrillar collagen, we again used our GFP–βPix knockdown/rescue fibroblasts to isolate collagen-specific βPix-binding proteins. We identified a collagen-specific interaction between βPix and protein phosphatase 2A (PP2A) through the regulatory subunit A α isoform (PPP2R1A) in both HFFs (Fig. 5f) and MDA-MB-231 cells (Supplementary Fig. 4h). PP2A can be activated specifically during migration in 3D collagen, but not fibronectin, through $\alpha_2\beta_1$ integrin[33]. To assess the role of PP2A in the βPix-collagen pathway, we used both siRNA against PPP2R1A and okadaic acid, a potent, specific inhibitor of PP2A activity[33]. Knocking down PPP2R1A with two independent siRNAs (Supplementary Fig. 5a,c–e) or treating HFFs with 1 nM okadaic acid (Supplementary Fig. 5b,f) revealed the same collagen-specific morphological and migratory defects mirroring βPix knockdown. Moreover, treatment of GFP–βPix knockdown/rescue cells migrating on fibrillar collagen with siRNA (Fig. 5g) or okadaic acid (Supplementary Fig. 5g) led to a direct increase in threonine phosphorylation on βPix in comparison with controls. To functionally link the association of βPix with PPP2R1A to reduced Thr 526 phosphorylation, we performed loss-of-function experiments by treating knockdown/rescue wild-type and T526A fibroblasts with PPP2R1A siRNA and assaying cell morphology and migration in 3D collagen. Knocking down PPP2R1A led to severe morphological and migratory defects in βPix KDR-WT fibroblasts; however, βPix KDR-T526A fibroblasts rescued the morphological phenotype and partially rescued the migratory defect resulting from PPP2R1A knockdown in 3D collagen (Supplementary Fig. 5h–j). These data indicate that PP2A is critical for regulating the absence of phosphorylation at Thr 526 on βPix during migration in fibrillar collagen environments.

Our findings establish that ECM-dependent regulation of a specific GEF is a fundamental mechanism governing migration in different microenvironments. We demonstrate that βPix is critical for efficient migration in fibrillar collagen environments by restraining RhoA signalling (Fig. 5h). Interestingly, this suppression occurs through a mechanism of Rho GTPase crosstalk between Cdc42 and RhoA that is regulated by a collagen-specific functional interaction between the GEF–GAP pair, βPix and srGAP1. Our model also suggests that binding of $\alpha_2\beta_1$ to fibrillar collagen leads, through PP2A, to loss of phosphorylation at Thr 526 on βPix and promotes association with srGAP1. Thr 526 is a phosphorylation site for Pak1 and PKA, and is implicated in Pak2 signalling[32,34]. Our observation of decreased

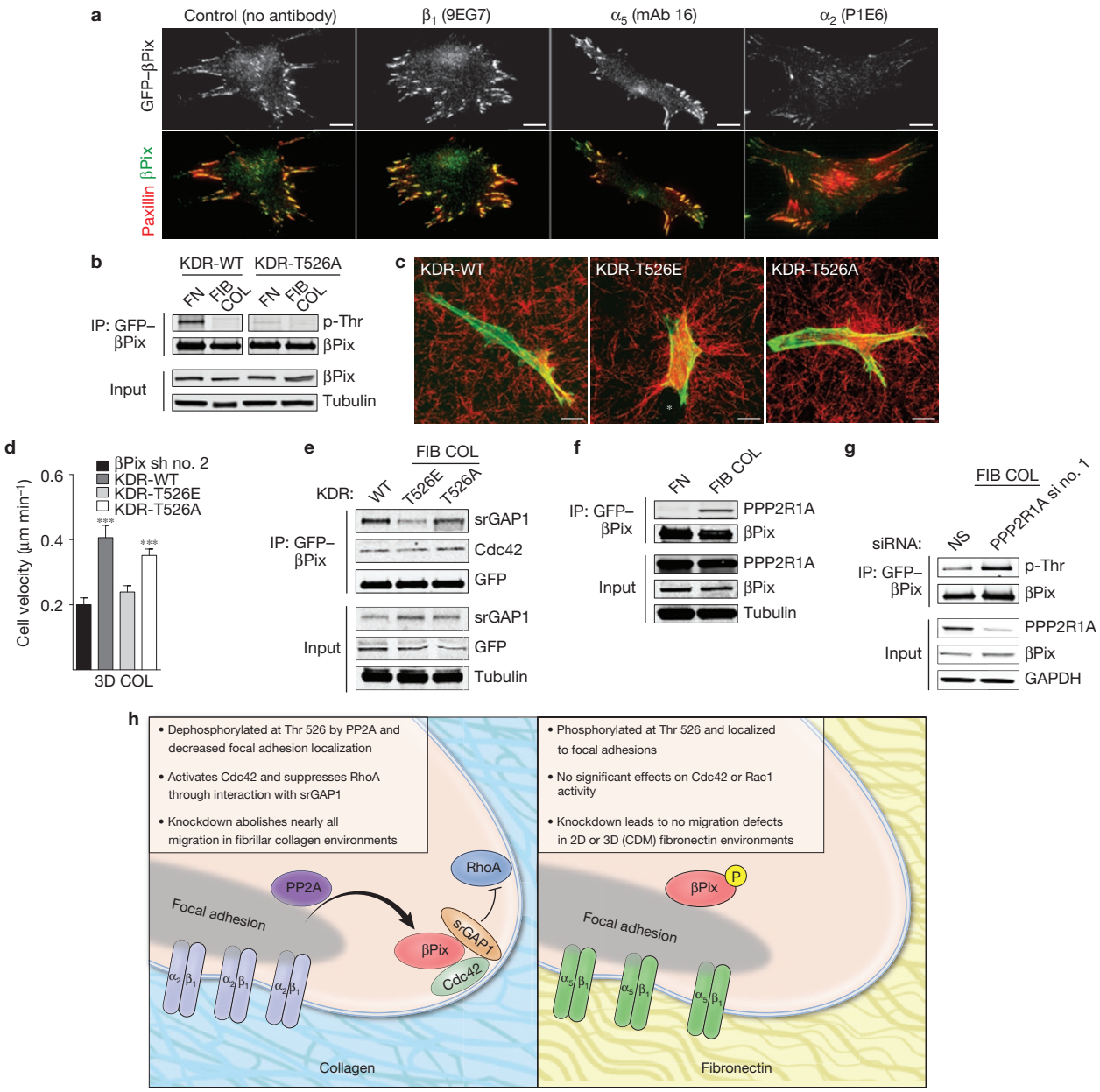

Figure 5 Fibrillar collagen activates βPix through $\alpha_2\beta_1$ integrin, leading to a critical dephosphorylation at Thr 526 through PP2A. (**a**) Loss of focal adhesion localization is a read-out of differential βPix function on fibrillar collagen (Fig. 1c). Dishes were coated with monoclonal integrin antibodies targeting β_1 (9EG7), α_5 (monoclonal antibody (mAb) 16) or α_2 (P1E6) to mimic integrin ligation. GFP–βPix knockdown/rescue cells were plated on the dishes and assayed for focal adhesion localization (red; yellow in overlay). Ligation of α_2 results in a marked loss in GFP–βPix (greyscale) localization at paxillin (red)-containing adhesions with no changes in overall focal adhesion profile. Scale bars, 25 μm. (**b**) Western blot of KDR-WT GFP–βPix immunoprecipitated from knockdown/rescue cells migrating on fibronectin or fibrillar collagen for phospho-threonine showed a decrease in phosphorylation levels during migration on collagen. Immunoprecipitation of KDR-T526A βPix showed no change in phospho-threonine between FN and FIB COL, highlighting the functional importance of this residue. (**c**) We generated phospho-mimetic (T526E) and phospho-null (T526A) mutant βPix knockdown/rescue cells and assayed their morphology in 3D collagen. T526E βPix was insufficient to rescue the morphological and hyper-contractile phenotype of βPix knockdown (collagen fibres, red, reflection microscopy). T526A mutants efficiently rescued the βPix morphological and contractile defects. Scale bars, 25 μm. (**d**) Quantification of cell velocity in βPix knockdown/rescue phosphovariants in 3D collagen. $n = 25$, 24, 22 and 22 cells for βPix sh no. 2, WT, T526E and T526A were assessed across three independent experiments (mean ± s.e.m., one-way ANOVA with Bonferroni multiple-comparison correction). (**e**) GFP–βPix was immunoprecipitated from HFFs expressing knockdown/rescue phosphovariants at Thr 526 migrating on fibrillar collagen. We find that the phosphorylation-mimetic (T526E) inhibits binding to srGAP1, but not Cdc42. (**f**) Immunoprecipitation of GFP–βPix from βPix knockdown/rescue cells migrating on fibronectin versus fibrillar collagen identified a collagen-specific interaction between βPix and the PP2A regulatory subunit A α isoform (PPP2R1A). (**g**) GFP–βPix knockdown/rescue fibroblasts migrating on fibrillar collagen were treated with NS or PPP2R1A siRNA no. 1. We observed that knockdown or inhibition (Supplementary Fig. 5g) of PPP2R1A increased phospho-threonine levels on βPix during migration on collagen. (**h**) Summary model of the collagen-specific role of βPix during migration in fibrillar collagen environments. All western blots are representative of at least three independent experiments. Statistical source data can be found in Supplementary Table 2; $^{***}P < 0.001$. Uncropped images of blots are shown in Supplementary Fig. 6.

association between βPix and Pak1 during migration in fibrillar collagen (Fig. 4b) may suggest that decreased activity of a kinase phosphorylating βPix could also contribute to regulating Thr 526 phosphorylation in response to fibrillar collagen.

Although there are many complex interactions and crosstalk events occurring at the leading edge of cells during migration, the βPix/srGAP1 complex provides an elegant mechanism for restricting RhoA and concentrating Cdc42 activity towards the leading edge in collagen microenvironments. We speculate that this and other potential specific GEF–GAP interactions could provide local contextual regulation in other ECM microenvironments that affects differentiation, morphogenesis, and tumour progression through RhoA signalling[7,35–38]. Our findings provide a mechanistic link between an external stimulus from collagen and regulation of Cdc42 and RhoA signalling during 3D cell migration. □

METHODS

Methods and any associated references are available in the online version of the paper.

Note: Supplementary Information is available in the online version of the paper

ACKNOWLEDGEMENTS

The authors would like to thank W. Daley, R. Petrie and D. Tran for critical reading of the manuscript. This study was supported by the Intramural Research Program of the National Institute of Dental and Craniofacial Research, NIH.

AUTHOR CONTRIBUTIONS

M.L.K. designed and carried out experiments. M.L.K. and K.M.Y. wrote the manuscript. K.M.Y. directed the project.

COMPETING FINANCIAL INTERESTS

The authors declare no competing financial interests.

Published online at www.nature.com/doifinder/10.1038/ncb3026
Reprints and permissions information is available online at www.nature.com/reprints

1. Friedl, P. & Wolf, K. Plasticity of cell migration: a multiscale tuning model. *J. Cell Biol.* **188,** 11–19 (2010).
2. Arthur, W. T., Noren, N. K. & Burridge, K. Regulation of Rho family GTPases by cell–cell and cell–matrix adhesion. *Biol. Res.* **35,** 239–246 (2002).
3. Petrie, R. J. & Yamada, K. M. At the leading edge of three-dimensional cell migration. *J. Cell Sci.* **125,** 5917–5926 (2012).
4. Guilluy, C., Garcia-Mata, R. & Burridge, K. Rho protein crosstalk: another social network? *Trends Cell Biol.* **21,** 718–726 (2011).
5. Doyle, A. D., Petrie, R. J., Kutys, M. L. & Yamada, K. M. Dimensions in cell migration. *Curr. Opin. Cell Biol.* **25,** 642–649 (2013).
6. Frantz, C., Stewart, K. M. & Weaver, V. M. The extracellular matrix at a glance. *J. Cell Sci.* **123,** 4195–4200 (2010).
7. Provenzano, P. P. *et al.* Collagen reorganization at the tumor-stromal interface facilitates local invasion. *BMC Med.* **4,** 38 (2006).
8. Daley, W. P. & Yamada, K. M. ECM-modulated cellular dynamics as a driving force for tissue morphogenesis. *Curr. Opin. Genet. Dev.* **23,** 408–414 (2013).
9. Petrie, R. J., Gavara, N., Chadwick, R. S. & Yamada, K. M. Nonpolarized signaling reveals two distinct modes of 3D cell migration. *J. Cell Biol.* **197,** 439–455 (2012).
10. Huttenlocher, A. & Horwitz, A. R. Integrins in cell migration. *Cold Spring Harb. Perspect. Biol.* **3,** a005074 (2011).
11. Petrie, R. J., Doyle, A. D. & Yamada, K. M. Random versus directionally persistent cell migration. *Nat. Rev. Mol. Cell Biol.* **10,** 538–549 (2009).
12. Raftopoulou, M. & Hall, A. Cell migration: Rho GTPases lead the way. *Dev. Biol.* **265,** 23–32 (2004).
13. Bos, J. L., Rehmann, H. & Wittinghofer, A. GEFs and GAPs: critical elements in the control of small G proteins. *Cell* **129,** 865–877 (2007).
14. Garcia-Mata, R. *et al.* Analysis of activated GAPs and GEFs in cell lysates. *Methods Enzymol.* **406,** 425–437 (2006).
15. Dubash, A. D. *et al.* A novel role for Lsc/p115 RhoGEF and LARG in regulating RhoA activity downstream of adhesion to fibronectin. *J. Cell Sci.* **120,** 3989–3998 (2007).
16. Pankov, R. *et al.* A Rac switch regulates random versus directionally persistent cell migration. *J. Cell Biol.* **170,** 793–802 (2005).
17. Kuo, J. C., Han, X., Hsiao, C. T., Yates, J. R. 3rd & Waterman, C. M. Analysis of the myosin-II-responsive focal adhesion proteome reveals a role for β-Pix in negative regulation of focal adhesion maturation. *Nat. Cell Biol.* **13,** 383–393 (2011).
18. Liu, F. *et al.* Cadherins and Pak1 control contact inhibition of proliferation by Pak1-βPIX-GIT complex-dependent regulation of cell-matrix signaling. *Mol. Cell. Biol.* **30,** 1971–1983 (2010).
19. Cau, J. & Hall, A. Cdc42 controls the polarity of the actin and microtubule cytoskeletons through two distinct signal transduction pathways. *J. Cell Sci.* **118,** 2579–2587 (2005).
20. Kutys, M. L., Doyle, A. D. & Yamada, K. M. Regulation of cell adhesion and migration by cell-derived matrices. *Exp. Cell Res.* **319,** 2434–2439 (2013).
21. Manser, E. *et al.* PAK kinases are directly coupled to the PIX family of nucleotide exchange factors. *Mol. Cell.* **1,** 183–192 (1998).
22. Lammermann, T. *et al.* Cdc42-dependent leading edge coordination is essential for interstitial dendritic cell migration. *Blood* **113,** 5703–5710 (2009).
23. Komatsu, N. *et al.* Development of an optimized backbone of FRET biosensors for kinases and GTPases. *Mol. Biol. Cell.* **22,** 4647–4656 (2011).
24. Yoshizaki, H. *et al.* Activity of Rho-family GTPases during cell division as visualized with FRET-based probes. *J. Cell Biol.* **162,** 223–232 (2003).
25. Ohta, Y., Hartwig, J. H. & Stossel, T. P. FilGAP, a Rho- and ROCK-regulated GAP for Rac binds filamin A to control actin remodelling. *Nat. Cell Biol.* **8,** 803–814 (2006).
26. Bustos, R. I., Forget, M. A., Settleman, J. E. & Hansen, S. H. Coordination of Rho and Rac GTPase function via p190B RhoGAP. *Curr. Biol.* **18,** 1606–1611 (2008).
27. Wong, K. *et al.* Signal transduction in neuronal migration: roles of GTPase activating proteins and the small GTPase Cdc42 in the Slit-Robo pathway. *Cell* **107,** 209–221 (2001).
28. Coutinho-Budd, J., Ghukasyan, V., Zylka, M. J. & Polleux, F. The F-BAR domains from srGAP1, srGAP2 and srGAP3 regulate membrane deformation differently. *J. Cell Sci.* **125,** 3390–3401 (2012).
29. Miyamoto, S. *et al.* Integrin function: molecular hierarchies of cytoskeletal and signaling molecules. *J. Cell Biol.* **131,** 791–805 (1995).
30. Mayhew, M. W. *et al.* Identification of phosphorylation sites in βPIX and PAK1. *J. Cell Sci.* **120,** 3911–3918 (2007).
31. Shin, E. Y. *et al.* Basic fibroblast growth factor stimulates activation of Rac1 through a p85 βPIX phosphorylation-dependent pathway. *J. Biol. Chem.* **279,** 1994–2004 (2004).
32. Chahdi, A., Miller, B. & Sorokin, A. Endothelin 1 induces β1Pix translocation and Cdc42 activation via protein kinase A-dependent pathway. *J. Biol. Chem.* **280,** 578–584 (2005).
33. Ivaska, J. *et al.* Integrin α2 β1 promotes activation of protein phosphatase 2A and dephosphorylation of Akt and glycogen synthase kinase 3 β. *Mol. Cell. Biol.* **22,** 1352–1359 (2002).
34. Koh, C. G., Manser, E., Zhao, Z. S., Ng, C. P. & Lim, L. β1PIX, the PAK-interacting exchange factor, requires localization via a coiled-coil region to promote microvillus-like structures and membrane ruffles. *J. Cell Sci.* **114,** 4239–4251 (2001).
35. Engler, A. J., Sen, S., Sweeney, H. L. & Discher, D. E. Matrix elasticity directs stem cell lineage specification. *Cell* **126,** 677–689 (2006).
36. Provenzano, P. P. *et al.* Collagen density promotes mammary tumor initiation and progression. *BMC Med.* **6,** 11 (2008).
37. Daley, W. P. *et al.* ROCK1-directed basement membrane positioning coordinates epithelial tissue polarity. *Development* **139,** 411–422 (2012).
38. Levental, K. R. *et al.* Matrix crosslinking forces tumor progression by enhancing integrin signaling. *Cell* **139,** 891–906 (2009).

DOI: 10.1038/ncb3026

METHODS

Cell lines and reagents. Primary human foreskin fibroblasts (HFFs), immortalized human fibroblasts (BJ5Ta and BR5, ATCC), human adenocarcinoma line MDA-MB-231, primary human osteoblasts (NhOst, Lonza), and HEK 293FT cells were cultured in phenol red-free DMEM (Hyclone) supplemented with 10% fetal bovine serum (Hyclone), 100 U ml^{-1} penicillin, 100 µg ml^{-1} streptomycin (Invitrogen) and 2 mM L-glutamine (Invitrogen) at 37 °C in 10% CO_2 in a humidified incubator. Human umbilical vein endothelial cells (HUVECs) and human aortic smooth muscle cells (AOSMCs, Lonza) were cultured in phenol red-free DMEM (Hyclone) supplemented with 5% fetal bovine serum (Hyclone), insulin, hFGF and hEGF (Lonza, SMGM-2 BulletKit) at 37 °C in 5% CO_2. The following reagents were used in this study: rhodamine– and Alexa488–phallodin (Invitrogen), cell-permeable C3 transferase (Cytoskeleton), blebbistatin and okadaic acid (EMD), and GFP-TRAP GFP-binding protein (Chromotek). GFP–RhoAQ63L was transfected into cells with the Nucleofector system (Lonza) using the NDHF kit (Lonza) according to the manufacturer's instructions. Equal concentrations of the dimethylsulphoxide vehicle were used as controls for drug studies.

Antibodies. The anti-βPix antibody (07-1450, 1:1,000), anti-GFP (3F8.2, 1:1,000), anti-PAK1 (EP656Y, 1:500), anti-Rac3 (07-2151, 1:500), anti-Rac2 (07-604, 1:500), and anti-PPPR2A1 (07-250, 1:1,000) were from Millipore. Anti-Rac1 (102, 1:1,000), anti-Cdc42 (44, 1:500) and anti-paxillin (349, 1:100) were from BD Biosciences. Anti-RhoA antibody (ab54835, 1:1,000) and anti-β tubulin (ab6046, 1:5,000) were from Abcam. Anti-p-threonine (42H4, 1:500) antibody was from Cell Signaling. Rabbit polyclonal antibody (5836, 1:2,500) against fibronectin was produced in-house. Anti-GAPDH (6c5, 1:5,000) was from Fitzgerald and anti-actin (AC-40, 1:1,000) was from Sigma. Anti-srGAP1 (286A, 1:500) was from Bethyl Laboratories, and anti-SmgGDS was from Novus Biologicals.

RNA-mediated interference. Individual ON-TARGETplus siRNAs against βPix, srGAP1, Rac3, Rac2 and PPP2R1A (Dharmacon-Thermo Scientific) and previously validated[9] Rho GTPase siRNAs against Rac1 and Cdc42 (Silencer Select, Invitrogen) were used for protein knockdown. All protein knockdowns were conducted with at least two independent RNAi sequences. For specific sequence information and labels see Supplementary Table 1. siRNAs were transfected into cells using Lipofectamine 2000 (Invitrogen) as previously described[9,16].

Lentiviral-mediated generation of stable fibroblast lines. Stable βPix knockdown and knockdown-rescue cells lines in primary HFFs were generated using the pLL 3.7 lentiviral packing system (11795, Addgene) as described previously[39]. Two independent shRNA hairpins targeting βPix regions: shRNA no. 2: 5′-GGAAGAAGATGCTCAGATT-3′ and shRNA no. 4: 5′-GTAGTAAGAGC AAAGTTTA-3′, along with a nonspecific control, 5′-GGAATCTCATTCGAT GCAT-3′, were cloned into the pLL3.7 lentiviral vector. For knockdown-rescue constructs, βPix cDNA (Origene) was cloned into pLL3.7 at the NheI–EcoRI restriction sites, creating C-terminal tagged GFP–βPix. The QuikChange Site-Directed Mutagenesis kit (Stratagene) was used to create three nucleotide substitutions that did not perturb the amino-acid sequence in βPix to generate a shRNA-resistant construct. In addition, similar mutagenesis techniques were used to introduce phospho-mimetic (KDR-T526E) and phospho-dead (KDR-T526A) mutations into βPix cDNA in the pLL 3.7 knockdown-rescue construct. GFP or mCherry-positive cells were isolated by fluorescence-activated cell sorting (BD FACS ARIA).

Purification of recombinant proteins. RacG15A and Cdc42G15A were cloned into pGEX4T-1 using the EcoRI–BamHI restriction sites. pGEX4T-1 constructs containing the Rho-binding domain (3× RBD) of Rhotekin cDNA was a gift from S. Gutkind (NIDCR, USA) and the p21-binding domain of Pak1 (PBD) was from Addgene (Plasmid 12217). Briefly, expression of the GST fusion proteins in *BL21 Escherichia coli* was induced with 200 µM isopropyl-β-D-thiogalactoside (IPTG) for 12–16 h at room temperature. Bacterial cells were lysed in buffer containing 20 mM HEPES pH 7.6, 1% Triton X-100, 150 mM NaCl, 5 mM $MgCl_2$, 1 mM dithiothreitol, protease and phosphatase inhibitor cocktails (Roche), and the proteins were purified by incubation with glutathione–Sepharose 4B beads (GE Healthcare) at 4 °C.

Mass spectrometry analysis. Single, excised Coomassie-stained bands for protein identification and phosphorylation analysis were analysed by MS Bioworks as follows. In-gel digestion was performed using a ProGest robot (DigiLab). Gel bands were washed with 25 mM ammonium bicarbonate followed by acetonitrile, reduced with 10 mM dithiothreitol at 60 °C followed by alkylation with 50 mM iodoacetamide at room temperature, digested with trypsin (Worthington) at 37 °C f or 4 h, and quenched with formic acid and the supernatant was analysed directly without further processing. Each digested sample was analysed by nano LC/MS/MS with a Waters NanoAcquity HPLC system interfaced to a ThermoFisher Q Exactive mass spectrometer. Thirty microlitres of sample was loaded on a trapping column and eluted over a 75 µm analytical column at 350 nl min^{-1}; both columns were packed with Jupiter Proteo resin (Phenomenex). The mass spectrometer was operated in data-dependent mode, with MS and MS/MS performed in the Orbitrap at 70,000 and 17,500 full-width at half-maximum resolution respectively. The 15 most abundant ions were selected for MS/MS. LC/MS/MS data were analysed using the MASCOT algorithm, with trypsin specified as the digestion enzyme (two max missed cleavages) and all data searched against the SwissProt Human database (forward and reverse appended with common contaminant proteins). Carbamidomethylation (C) was set as a fixed modification. For protein identification, Oxidation (M), Acetyl (N-term), Pyro-Glu (N-term Q), Deamidation (N,Q) were selected as variable. For phosphoanalysis, the same modifications were variable, in addition to Phospho (S-T-Y). Peptide mass tolerances were set to 10 ppm and fragment mass tolerance was set to ±0.015 Da. Mascot DAT files were parsed into the Scaffold software for validation, filtering and to create a non-redundant list per sample. The data were filtered using a minimum protein value of 80%, and a minimum peptide value of 50% (Prophet scores).

GEF activity and GTPase activity affinity assays. GST–RacG15A active GEF-pulldown experiments were carried out as described previously[14,15]. Dishes were coated with 10 µg ml^{-1} human plasma-derived fibronectin or 50 µg ml^{-1} rat tail type I collagen overnight at 4 °C. HFFs were serum starved for 2 h before plating, then plated in serum-free DMEM and allowed to reach steady-state migration over 12–16 h. Cells were lysed in 20 mM HEPES pH 7.6, 1% Triton X-100, 150 mM NaCl, 5 mM $MgCl_2$, 1 mM dithiothreitol, protease and phosphatase inhibitor cocktails (Roche) and sonicated at 3 W on ice for 5 s at 4 °C using a Misonix Microson XL sonicator. Lysates adjusted to equal quantities and concentrations of protein were incubated with 25 µg of purified GST–RacG15A or GST–Cdc42G15A for 1 h at 4 °C. Samples were washed in lysis buffer (3 times for western blotting or 5 times for mass spectrometry) and analysed by SDS–PAGE using Novex Tris-Glycine 4–12% polyacrylamide gels (Invitrogen). For identification of the GEFs bound to RacG15A by mass spectrometry, SDS–PAGE gels were Coomassie-stained with GelCode Blue Stain Reagent (Pierce). Bands of interest were extracted and identified using nano LC/MS/MS (MS Bioworks). For active RhoA, Cdc42 and Rac1 pulldowns, plates and cells were prepared as indicated above. Fibroblasts that were cultured overnight in complete media (RhoA) or serum-free media (Rac1, Cdc42) were lysed in 50 mM Tris pH 7.6, 200 mM NaCl, 1% Triton X-100, 0.5% deoxycholate, 5 mM $MgCl_2$, and protease and phosphatase inhibitor cocktails, sonicated at 3 W on ice for 5 s, and clarified at 12,000*g* for 5 min. Lysates were equalized for protein content and volume and rotated at 4 °C for 1 h with either 20 µg GST–RBD or 30 µg GST–PBD. Bead pellets were washed three times with lysis buffer and analysed by SDS–PAGE as described above. Polyacrylamide gels were transferred to nitrocellulose membranes using the semi-dry iBlot transfer system (Invitrogen). Membranes were blocked with Odyssey blocking buffer (LI-COR) for 1 h at room temperature. Primary antibodies were incubated with membranes in Odyssey blocking buffer containing 0.1% Tween-20 overnight at 4 °C. Membranes were washed with TBS containing 0.1% Tween-20 (TBST) three times over 30 min. IRDye-conjugated anti-mouse and rabbit secondary antibodies (1:20,000) (LI-COR) were incubated in Odyssey blocking buffer containing 0.1% Tween-20 for 30 min at room temperature. Membranes were then washed with TBS containing 0.1% Tween-20 (TBST) three times over 30 min. All western blots were imaged and quantified using the Odyssey imaging system through the analyse module (LI-COR). Intensity values were normalized to load control (tubulin or GAPDH).

Membrane fractionation and immunoprecipitation. For Triton X-100 membrane fractionation, cells cultured on a matrix overnight in complete media were lysed in 50 mM Tris pH 7.6, 150 mM NaCl, 1% Triton X-100, and protease and phosphatase inhibitor cocktails. Lysates were vortexed and incubated by end-over-end rotation for 20 min at 4 °C. Cell lysates were fractionated by centrifuging at 15,500*g* for 15 min. The resulting pellets (insoluble fraction) were washed three times with lysis buffer and then denatured in 2× Novex sample buffer (Invitrogen) containing 100 µM dithiothreitol for 5 min at 95 °C. Pellets were compared with supernatant (soluble fraction) by SDS–PAGE using Novex Tris-glycine 4–12% polyacrylamide gels (Invitrogen). For immunoprecipitation of GFP–βPix from fibrillar collagen environments, cells cultured on a matrix overnight in complete media were lysed in 50 mM Tris pH 7.6, 200 mM NaCl, 1% Triton X-100, 0.5% deoxycholate, 5 mM $MgCl_2$, and protease and phosphatase inhibitor cocktails (Roche), homogenized using 200–1,000 µl positive displacement pipettes (Anachem), sonicated at 3 W on ice for 3 s, and incubated for 7 min with end-over-end rotation at 4 °C. Lysates were clarified by centrifugation at 12,000*g*, equalized for protein content and volume, and incubated for 1 h with 30 µl of GFP-TRAP (Chromotek) conjugated to magnetic beads at 4 °C with end-over-end rotation. For mass spectrometry analysis, beads were washed five times with

lysis buffer and analysed by SDS–PAGE and Coomassie blue staining. For the identification of srGAP1, excised gel bands were analysed using nano LC/MS/MS (MS Bioworks).

Generation of cell-derived matrices. Cell-derived matrices (CDMs) were prepared from HFFs as described previously[9]. MatTek dishes were coated with 0.2% gelatin for 1 h at 37 °C, treated with 1% glutaraldehyde for 30 min at room temperature, and incubated with DME for 30 min at room temperature. Three washes with Dulbecco's PBS with calcium and magnesium (PBS+) followed each treatment. HFFs were plated at 4×10^5 per MatTek dish, and were maintained for 10 d, adding fresh media with 50 μg ml^{-1} ascorbic acid every other day. The cells were removed from the CDM with extraction buffer (20 mM NH_4OH and 0.5% Triton X-100 in PBS+) for 5 min at room temperature and washed with PBS+. The cell-free CDM was treated with 10 U ml^{-1} DNase (Roche) for 30 min at 37 °C, washed with Dulbecco's PBS without calcium and magnesium (PBS), and stored at 4 °C in PBS with 100 U ml^{-1} penicillin and 100 μg ml^{-1} streptomycin.

Generation of fibrillar collagen matrices and time-lapse microscopy. Fibrillar collagen gel solutions (2 mg ml^{-1}) were prepared by mixing rat tail type I collagen with 10× reconstitution buffer (0.26 M $NaHCO_3$ and 0.2 M HEPES) and 10× DME (Sigma), adjusting the pH to 7.4 with 1 M NaOH, and then diluting to 2 mg ml^{-1} with PBS+. To generate thin fibrillar collagen substrates, 30 μl of solution was spread on a 20 mm MatTek dish and allowed to polymerize for 1 h at room temperature. Using these substrates for biochemical assays facilitated cellular extraction and minimized collagen contamination in comparison with 3D collagen. In addition, these substrates minimized light scatter during imaging and provided the fibrillar collagen substrate required for the βPix knockdown phenotype. Fibroblasts were plated in complete medium overnight and assayed for motility the following day. For 3D collagen gels, cells were resuspended in PBS+ and mixed with the prepared collagen mixture. The collagen–cell mixture was spread on MatTek dishes and allowed to polymerize at room temperature for 1 h. Complete medium was added to the gels, and the cells were assayed for motility the next day. For phase-contrast microscopy time-lapse imaging of fibroblasts in different matrix environments, complete medium was added before image acquisition. For inhibitor treatments, vehicle control or inhibitors were incubated with cells for 4–6 h before beginning the time-lapse imaging. Random cell migration was imaged for 24 h in 37 °C, 10% CO_2 environmental chambers. Time-lapse videos were recorded on a microscope (Axiovert 135TV; Carl Zeiss) fitted with a motorized *xy*- and *z*-stage focus drive (Ludl Electronic Products) using an enhanced contrast Plan-Neofluar ×10 0.3 NA or a long-working distance Plan-Neofluar Korr ×20 0.4 NA objective (Carl Zeiss). Images were acquired with a charge-coupled device camera (ORCA II ER; Hamamatsu Photonics). Microscopy images were adjusted for brightness and contrast and cells were tracked manually using MetaMorph software.

Live-cell fluorescence and FRET imaging. Fibroblasts were imaged with a modified Yokogawa spinning-disc confocal scan head (CSU-21: modified by Spectral Applied Research) attached to an automated Olympus IX-81 microscope using a ×60 SAPO-Chromat silicone oil objective (N.A. 1.3). A custom laser launch equipped with 442 nm (40 mW: Melles Griot), 488 nm (150 mW: Coherent), 514 nm (150 mW: Coherent), 568 nm (100 mW: Coherent) and 642 nm (110 mW: Vortran) diode lasers supplied excitation wavelengths. A Gooch and Housego AOTF controlled shuttering and intensity for 488, 514 and 568 laser lines. The 442 and 642 lines were shuttered and intensity controlled through TTL and direct voltage steps, respectively. The primary dichroics (442/568/647 and 405/488/568/647) were from Semrock. Images were captured using a backthinned electron-multiplying CCD (charge-coupled device) camera in 16-bit format using the 10 MHz digitization setting (Roper Scientific).

mCherry was cloned into pLL3.7 in place of GFP to allow FRET compatibility. mCherry-βPix knockdown fibroblasts were generated with the shRNA no. 2 hairpin. The binding of active Cdc42 or RhoA was detected by imaging the FRET-dependent, intramolecular emission fluorophore (YPet) from YPet–PAK–EV–Cdc42–CFP or YPet–RBD–EV–RhoA–CFP (ref. 24) (kind gifts from M. Matsuda, Kyoto University, Japan.). Fibroblasts were transfected as indicated using the Nucleofector system (Amaxa) according to the manufacturer's instructions. The next day, cells were trypsinized and plated onto fibronectin or fibrillar collagen matrices in complete media and allowed to adhere overnight. Cells were imaged the following morning in 5% fetal bovine serum, phenol-red free DMEM with 10 units ml^{-1} Oxyrase. Optimal FRET acquisition settings were determined for the Olympus IX-81 spinning-disc microscope and strictly maintained during all subsequent FRET imaging; intensity levels of biosensor expression were similarly carefully controlled and maintained between selected cells. Ratio FRET images were obtained as previously described[40]. Images of CFP and YPet were obtained for each z-plane under 442 nm illumination. Maximum projections of confocal *z*-stacks were generated using MetaMorph software. Images were first background subtracted and a binary mask was applied by thresholding to the cytoplasmic mCherry–lentiviral marker to isolate the cellular signal. FRET ratio images were generated in MetaMorph using the arithmetic module, with a universally applied scaling factor of 1,000. All resulting FRET images were processed with a 3 × 3 median filter to remove any hot pixels and presented in a pseudocolour map (MetaMorph). The same pseudocolour intensity scale was maintained for each ECM condition for the NS and βPix shRNA conditions. Polarization index (PI) was calculated as previously described[9] using the five highest points of FRET intensity per cell analysed. A PI of 1 = forward polarization, 0 = nonpolarization (regions are uniformly distributed), and −1 = rearward polarization.

Immunofluorescence. For morphological analysis in 3D collagen or CDM and immunolocalization of Cdc42, cells cultured in complete medium were fixed with 4% paraformaldehyde in PBS+, permeabilized with 0.25% Triton X-100 in PBS+, and blocked with 1% BSA in PBS+. Rhodamine– or Alexa488–phalloidin and primary and secondary antibodies were applied in 1% BSA in PBS+ and samples were rinsed with PBS+ three times over 30 min between each treatment. The elliptical factor was calculated as the ratio of cell length to cell width at maximal points in 3D reconstructions using MetaMorph software. For localization analysis of βPix to focal adhesions on fibrillar collagen, cells were fixed-permeabilized with 3% paraformaldehyde–0.5% Triton X-100 in PBS+ at 37 °C followed by an additional fixation with 4% paraformaldehyde. Cells were blocked with 1% BSA in PBS+. Primary and secondary antibodies were applied in 1% BSA in PBS+ and rinsed three times over 30 min with PBS+ between each treatment. For all confocal microscope immunofluorescence analyses, cells were imaged with the same Yokogawa CSU-21/Olympus IX-81 spinning-disc microscope listed for live-cell imaging with a ×60 SAPO-Chromat silicone oil objective (N.A. 1.3) for morphological imaging and a Plan Apo N ×150 1.45 NA objective (TIRFM UIS2; Olympus) for βPix localization imaging. For analysis of βPix localization to focal adhesions after plating of cells on monoclonal integrin antibodies, dishes were coated with poly-L-lysine for 10 min at room temperature, washed with PBS+, and incubated with each antibody in PBS+ for 1 h at 37 °C. Dishes were washed three times with PBS+ and blocked for a further hour at 37 °C with 1% BSA. GFP–βPix KDR (knockdown-rescue) cells were plated in complete media overnight. The next day, the same fix-permeabilization methodology was used as described above. Cells were imaged using TIRF microscopy, performed using an Olympus IX-71 microscope using a Plan Apo N ×60 1.45 NA objective (TIRFM UIS2; Olympus). Fluorescence images were adjusted for brightness and contrast using MetaMorph software.

Statistical analysis. When experiments involved only a single pair of conditions, statistical differences between the two sets of data were analysed with a two-tailed, unpaired Student *t*-test with Prism5 (GraphPad Software). For data sets containing more than two samples, one-way ANOVA with a classical Bonferroni multiple-comparison post-test was used to determine adjusted *P* values. Sample sizes of sufficient power were chosen on the basis of similar published research and were confirmed statistically by appropriate tests. Experiments were not randomized. However, the investigator was blinded during the assessment of key morphological and migratory experiments involving βPix, Cdc42, Rac1 and srGAP1 knockdowns under different matrix conditions by using randomization of data labels. Primary statistics source data for all main and supplementary figures are available in Supplementary Table 2. Statistically significant differences are reported at *, $P < 0.05$, **, $P < 0.01$ and ***, $P < 0.001$.

39. Cai, L., Marshall, T. W., Uetrecht, A. C., Schafer, D. A. & Bear, J. E. Coronin 1B coordinates Arp2/3 complex and cofilin activities at the leading edge. *Cell* **128,** 915–929 (2007).
40. Hodgson, L., Shen, F. & Hahn, K. Biosensors for characterizing the dynamics of rho family GTPases in living cells. *Curr. Protoc. Cell Biol.* **46,** 14.11.1–14.11.26 (2010).

nature cell biology

DOI: 10.1038/ncb3026

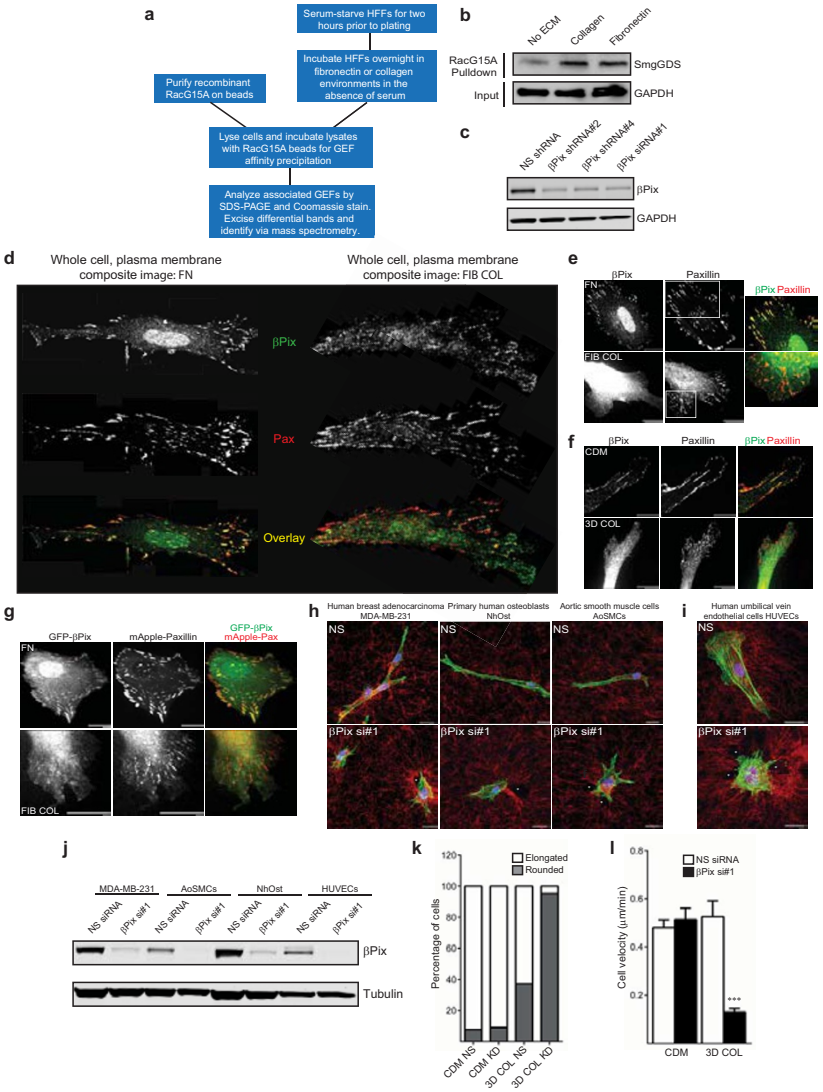

Supplementary Figure 1 (**a**) Schematic diagram of the screen for ECM-specific GEFs. Briefly, HFFs were plated on ECM-coated dishes, allowed to reach steady-state migration overnight in the absence of serum, lysed, and incubated with GST-RacG15A conjugated to beads to extract active GEFs. Beads were analyzed by SDS-PAGE, Coomassie staining, and mass spectrometry of excised protein bands for identification. (**b**) Western blot confirms up-regulation of SmgGDS binding to RacG15A in the presence of collagen or fibronectin (result was confirmed with three independent experiments). (**c**) Knockdown of βPix was achieved by generating HFF lines stably expressing either NS shRNA or two βPix shRNA hairpins (shRNA#2 or shRNA#4). Migration experiments were performed using each hairpin and a single siRNA toward βPix, resulting in identical phenotypes. (**d**) In maximum intensity confocal projections showing all βPix in a cell, the strong nuclear/intracellular membrane localization on both fibronectin and collagen substrates obscures the unique membrane localization in each ECM condition (e.g. Supplementary Fig.1e). Consequently, we focused on the single confocal section showing plasma membrane-localized βPix (green) and paxillin (red) using composite images at the plasma membrane plane of HFFs migrating on fibronectin (5 image segments in these relatively flat cells) or fibrillar collagen (21 image segments) of 0.2 μm confocal slices to visualize βPix localization at the cell-ECM interface. On fibronectin, βPix was concentrated in focal adhesions (yellow co-localization) with the nuclear staining visible because the cells were flatter. On fibrillar collagen, βPix was uniformly distributed along the plasma membrane with distinct, non-paxillin containing aggregates (green) observed toward the leading edge; nuclear staining was not in the plane of the plasma membrane in these less-flat cells. (**e**) Maximum confocal projections of βPix (green) and paxillin (red) in fibroblasts migrating on FN and FIB COL. Scale bars, 25 μm. (**f**) HFFs in 3D collagen and 3D CDM immunostained for endogenous paxillin (red) and βPix (green) display the same loss of adhesion localization as observed on fibronectin and fibrillar collagen (Fig. 1c); yellow indicates co-localization. Scale bars, 25 μm. (**g**) Live GFP-βPix knockdown/rescue cells expressing mApple-paxillin (red) migrating on fibronectin or fibrillar collagen display loss of adhesion localization; yellow indicates co-localization. Scale bars, 25 μm. (**h**) Single siRNA knockdown of βPix in human breast adenocarcinoma cells, primary human osteoblasts, human aortic smooth muscle cells, and human umbilical vein endothelial cells revealed collagen-specific morphological and migratory defects between 3D collagen and 3D cell-derived matrix (data not shown for CDM) and (**i**) 2D fibronectin and fibrillar collagen (green, actin; red, collagen). (**j**) Western blot confirmation of βPix knockdown using a single βPix siRNA. (**k**) Quantification of morphology of MDA-MB-231 cells with βPix knockdown in 3D collagen versus 3D cell-derived matrix. Elongated cells defined as having an elliptical factor > 1.5. n = 30, 30, 26, and 27 cells for CDM NS, CDM KD, COL NS, and COL KD were assessed across three independent experiments (mean ± s.e.m., *t*-tests). (**l**) Quantification of MDA-MB-231 cell velocity with βPix knockdown in 3D cell-derived matrix or 3D collagen. n = 19, 19, 19, and 21 cells for NS CDM, βPix si#1 CDM, NS COL, and βPix si#1 COL were assessed across three independent experiments (mean ± s.e.m., *t*-tests). Statistical source data can be found in Supplementary Table 2. *** $P < 0.001$.

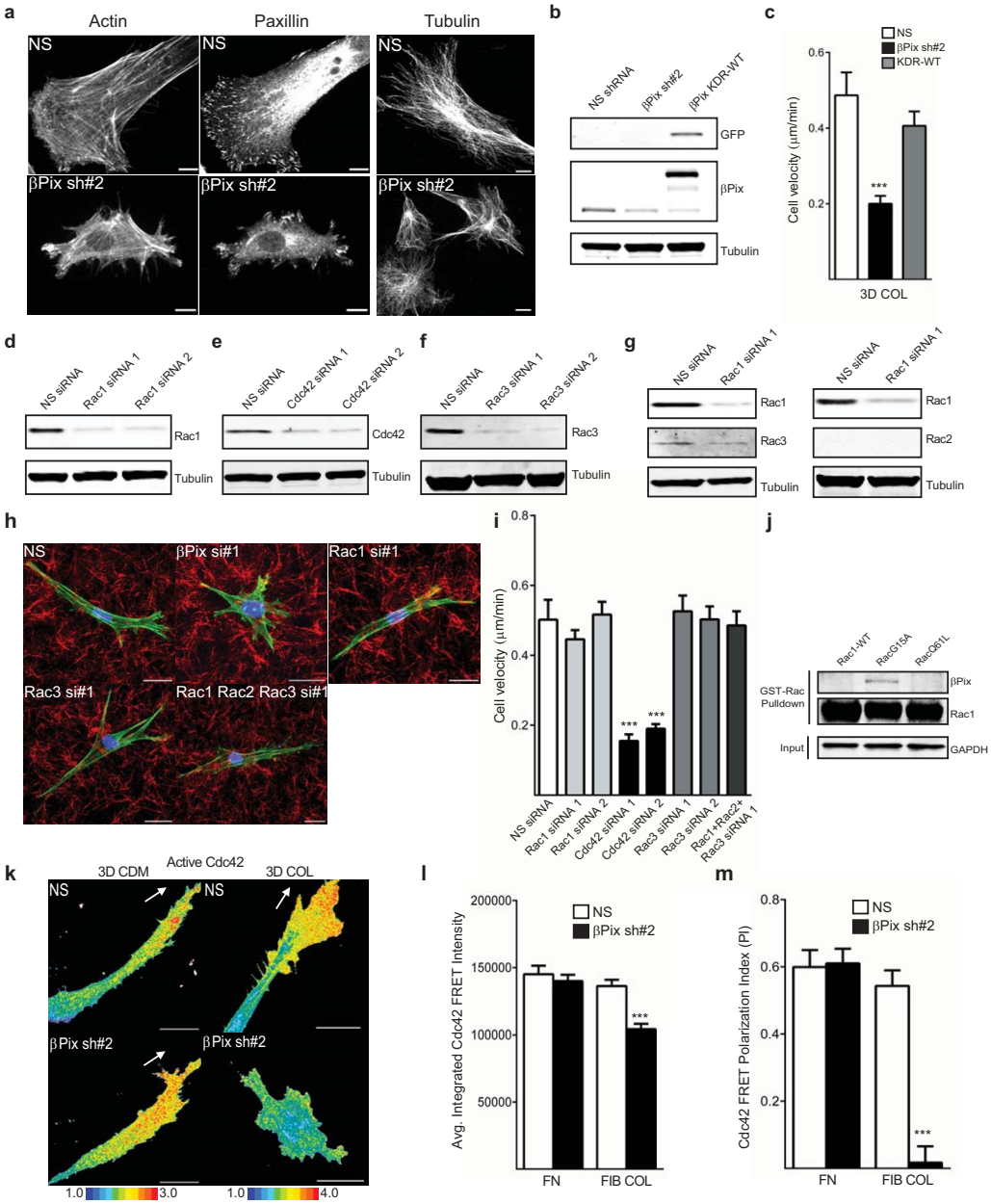

Supplementary Figure 2 (**a**) Immunostaining of endogenous paxillin, actin, and β-tubulin in HFFs on fibrillar collagen expressing NS or βPix shRNA. The multiple protrusions in βPix knockdown cells have paxillin-containing adhesions, enriched actin fibers, and efficient microtubule targeting. Scale bars, 20 μm. (**b**) Western blot of fibroblasts expressing NS shRNA, βPix shRNA#2, or βPix knockdown with a GFP-βPix rescue (βPix KDR-WT). GFP marker indicates the successful expression of the rescue construct at near endogenous levels. (**c**) Quantification of cell velocity of fibroblasts expressing NS shRNA, βPix shRNA, or βPix knockdown/rescue constructs in 3D collagen. n = 25, 24, and 25 cells for NS, βPix sh#2, and KDR-WT were assessed across three independent experiments (mean ± s.e.m., one-way ANOVA with Bonferroni correction). Single siRNA knockdown controls toward (**d**) Rac1, (**e**) Cdc42, and (**f**) Rac3. HFFs do not express Rac2. (**g**) Knockdown of Rac1 led to no compensatory increase in Rac3 (left) or Rac2 (right) protein levels. (**h**) Max projections of phalloidin stained HFFs in 3D collagen treated with single siRNAs toward βPix, Rac1, Rac3, or Rac1, Rac2 and Rac3. No Rac siRNA treatment was capable of recapitulating the βPix knockdown morphological phenotype. Scale bars, 25 μm (**i**) Quantification of migration velocities of GTPase siRNA-treated HFFs in 3D collagen. Two independent siRNAs toward Cdc42 mimic βPix knockdown. Additionally, Rac1 and Rac3 knockdown had no significant effect on HFF migration in 3D collagen. n = 18-25 cells for NS, Rac1 #1, Rac1 #2, Cdc42 #1, Cdc42 #2, Rac3 #1, Rac3 #2, and Rac1-3 #1 siRNAs were assessed across three independent experiments (mean ± s.e.m., one-way ANOVA with Bonferroni correction. (**j**) βPix specifically binds dominant negative RacG15a and not wild-type Rac1 or constitutively active Rac1 (Q61L) in lysates extracted from cells migrating on collagen. (**k**) Maximum projections of confocal stacks of live-fibroblast migration expressing a Cdc42 biosensor in 3D cell-derived matrix or 3D collagen. Knockdown of βPix in 3D leads to collagen-specific decreases in Cdc42 activity and loss of leading edge polarization. Scale bars, 25 μm. (**l**) Average integrated whole cell Cdc42 FRET intensity on FN versus FIB COL. n = 10 cells for NS FN, βPix sh#2 FN, NS FIB COL, and βPix sh#2 FIB COL were assessed across three independent experiments (mean ± s.e.m., *t*-test). (**m**) Quantification Cdc42 FRET polarization index on FN versus FIB COL. n = 10 cells for NS FN, βPix sh#2 FN, NS FIB COL, and βPix sh#2 FIB COL were assessed across three independent experiments (mean ± s.e.m., *t*-test). Statistical source data can be found in Supplementary Table 2. *** $P < 0.001$

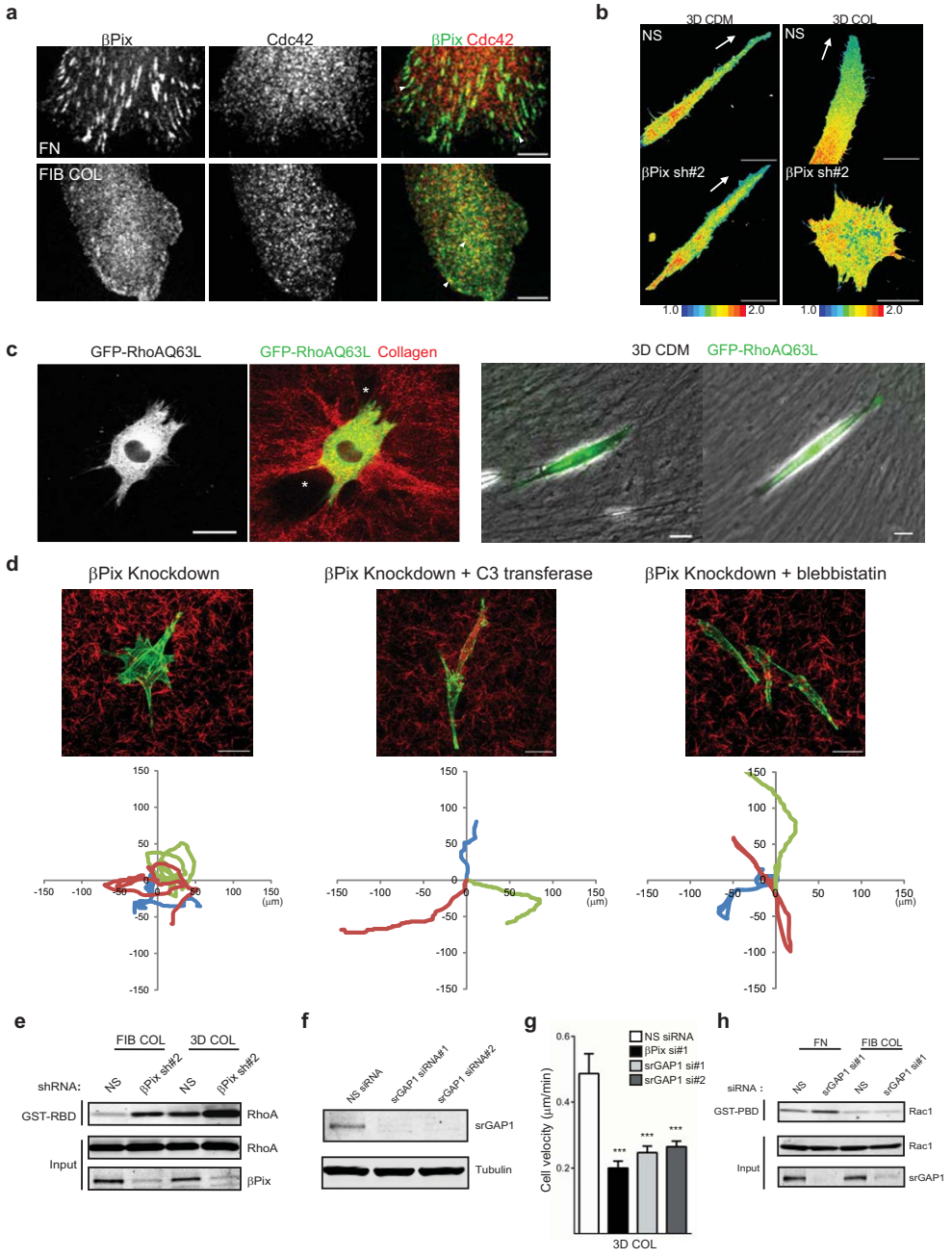

Supplementary Figure 3 (**a**) Immunostaining of βPix (green) and Cdc42 (red) at the leading edge of HFFs on fibronectin or fibrillar collagen. Migration on fibrillar collagen revealed increased but partial co-localization between βPix and Cdc42 (yellow, white arrows) in comparison to cells on fibronectin Scale bars, 10 μm. (**b**) Maximum projections of confocal stacks of live-fibroblast migration expressing a RhoA biosensor in 3D cell-derived matrix or 3D collagen. Knockdown of βPix in 3D leads to similar collagen-specific increases in RhoA activity and loss of front-back polarization of RhoA activity. Scale bars, 25 μm. (**c**) Low-level overexpression of GFP-RhoAQ63L (grayscale, green) during 3D collagen migration (left). We find that similar to βPix and Cdc42 knockdown, RhoAQ63L leads to a rounded, notably hyper-protrusive cell with significant remodeling of collagen fibers (red; holes in the collagen matrix, white asterisks). Expressing RhoAQ63L at comparable levels in HFFs migrating in cell-derived matrix (right) does not perturb morphology or lead to hyper-protrusive behaviors. Scale bar, 25 μm. (**d**) Max projections of phalloidin-stain (green) βPix knockdown cells in 3D collagen (red) treated with inhibitors of RhoA (cell-permeable C3 transferase, 2 μg/ml) or myosin II (blebbistatin, 20 μM) (top). Representative migratory tracks of each condition. We find that direct inhibition of RhoA with C3 transferase significantly rescues the motility of βPix knockdown, while blebbistatin rescues to a lesser degree (bottom). (**e**) RhoA activity determined using GST-RBD binding from NS and βPix shRNA-expressing fibroblasts migrating in 3D or fibrillar collagen environments. Representative of three independent experiments. (**f**) Single siRNA knockdown controls toward srGAP1. (**g**) Quantification of migration velocities of srGAP1 siRNA-treated HFFs in 3D collagen. 21, n = 24, 22, and 19 cells for NS, βPix si#1, srGAP1 si#1, and srGAP1 si#2 were assessed across three independent experiments (mean ± s.e.m., one-way ANOVA with Bonferroni correction). (**h**) srGAP1 has been reported to have GAP activity toward Rac1. Active Rac1 was isolated using GST-PBD from NS and srGAP1 siRNA-treated fibroblasts migrating on fibronectin (FN) or fibrillar collagen (FIB COL). Confirming previous reports, we observed an increase in Rac1 activity with srGAP1 knockdown during migration on fibronectin, but not during collagen migration. Blot representative of two independent experiments. Statistical source data can be found in Supplementary Table 2, *** $P < 0.001$.

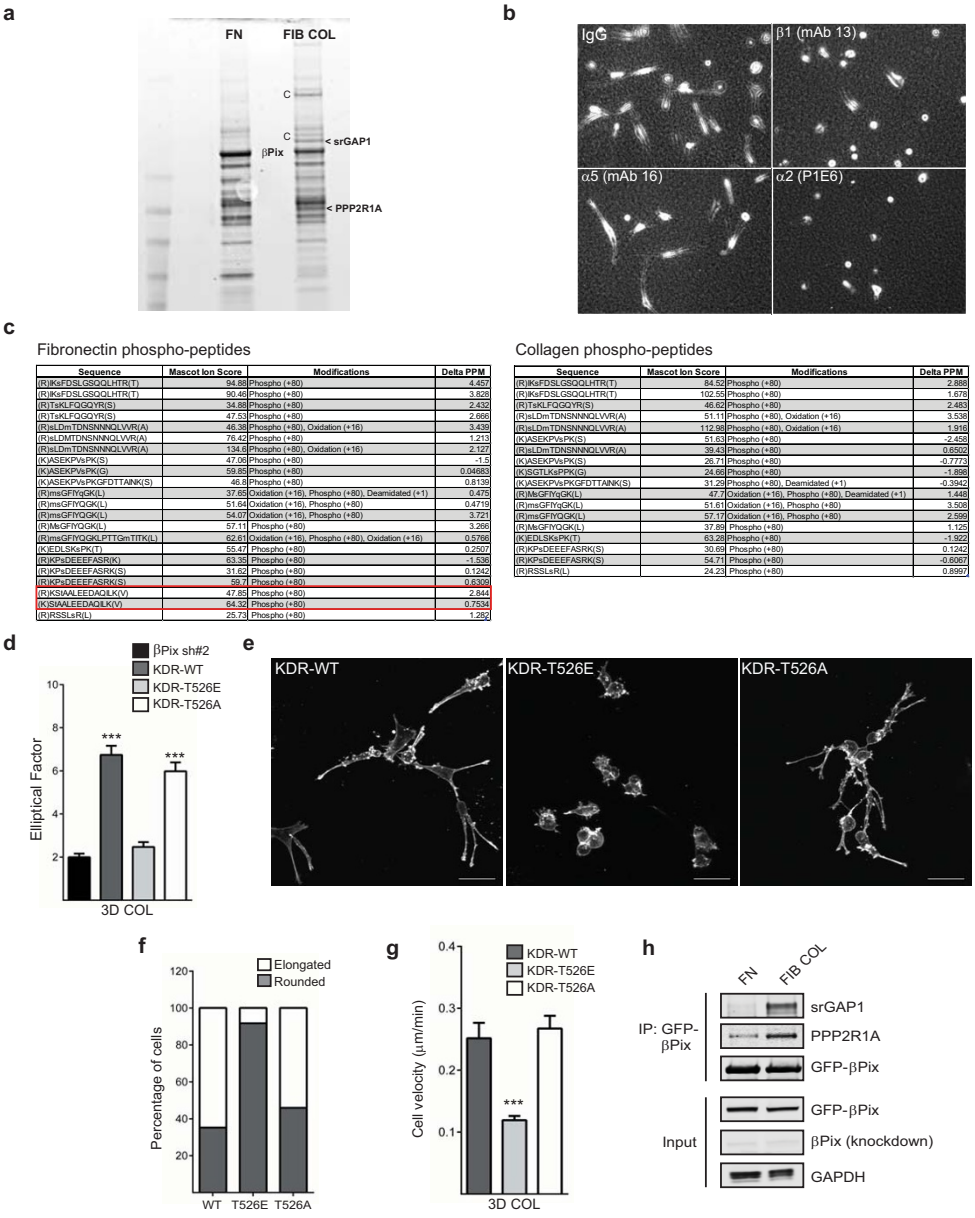

Sequence	Mascot Ion Score	Modifications	Delta PPM
(R)IKsFDSLGSQQLHTR(T)	94.88	Phospho (+80)	4.457
(R)IKsFDSLGSQQLHTR(T)	90.46	Phospho (+80)	3.828
(R)TsKLFQGQYR(S)	34.88	Phospho (+80)	2.432
(R)TsKLFQGQYR(S)	47.53	Phospho (+80)	2.666
(R)sLDmTDNSNNNQLVVR(A)	46.38	Phospho (+80), Oxidation (+16)	3.439
(R)sLDMTDNSNNNQLVVR(A)	76.42	Phospho (+80)	1.213
(R)sLDmTDNSNNNQLVVR(A)	134.6	Phospho (+80), Oxidation (+16)	2.127
(K)ASEKPVsPK(S)	47.06	Phospho (+80)	-1.5
(K)ASEKPVsPK(G)	59.85	Phospho (+80)	0.04683
(K)ASEKPVsPKGFDTTAINK(S)	46.8	Phospho (+80)	0.8139
(R)msGFIYqGK(L)	37.65	Oxidation (+16), Phospho (+80), Deamidated (+1)	0.475
(R)msGFIYQGK(L)	51.64	Oxidation (+16), Phospho (+80)	0.4719
(R)msGFIYQGK(L)	54.07	Oxidation (+16), Phospho (+80)	3.721
(R)MsGFIYQGK(L)	57.11	Phospho (+80)	3.266
(R)msGFIYQGKLPTTGmTITK(L)	62.61	Oxidation (+16), Phospho (+80), Oxidation (+16)	0.5766
(K)EDLSKsPK(T)	55.47	Phospho (+80)	0.2507
(R)KPsDEEEFASR(K)	63.35	Phospho (+80)	-1.536
(R)KPsDEEEFASRK(S)	31.62	Phospho (+80)	0.1242
(R)KPsDEEEFASRK(S)	59.7	Phospho (+80)	0.6309
(R)KStAALEEDAQILK(V)	47.85	Phospho (+80)	2.844
(K)StAALEEDAQILK(V)	64.32	Phospho (+80)	0.7534
(R)RSSLsR(L)	25.73	Phospho (+80)	1.282

Sequence	Mascot Ion Score	Modifications	Delta PPM
(R)IKsFDSLGSQQLHTR(T)	84.52	Phospho (+80)	2.888
(R)IKsFDSLGSQQLHTR(T)	102.55	Phospho (+80)	1.678
(R)TsKLFQGQYR(S)	46.62	Phospho (+80)	2.483
(R)sLDmTDNSNNNQLVVR(A)	51.11	Phospho (+80), Oxidation (+16)	3.538
(R)sLDmTDNSNNNQLVVR(A)	112.98	Phospho (+80), Oxidation (+16)	1.916
(K)ASEKPVsPK(S)	51.63	Phospho (+80)	-2.458
(R)sLDmTDNSNNNQLVVR(A)	39.43	Phospho (+80)	0.6502
(K)ASEKPVsPK(S)	26.71	Phospho (+80)	-0.7773
(K)SGTLKsPPK(G)	24.66	Phospho (+80)	-1.898
(K)ASEKPVsPKGFDTTAINK(S)	31.29	Phospho (+80), Deamidated (+1)	-0.3942
(R)MsGFIYqGK(L)	47.7	Oxidation (+16), Phospho (+80), Deamidated (+1)	1.448
(R)msGFIYqGK(L)	51.61	Oxidation (+16), Phospho (+80)	3.508
(R)msGFIYQGK(L)	57.17	Oxidation (+16), Phospho (+80)	2.599
(R)MsGFIYQGK(L)	37.89	Phospho (+80)	1.125
(K)EDLSKsPK(T)	63.28	Phospho (+80)	-1.922
(R)KPsDEEEFASRK(S)	30.69	Phospho (+80)	0.1242
(R)KPsDEEEFASRK(S)	54.71	Phospho (+80)	-0.6067
(R)RSSLsR(L)	24.23	Phospho (+80)	0.8997

Supplementary Figure 4 (**a**) GFP-βPix knockdown/rescue cells were allowed to reach steady-state migration on fibronectin (FN) or fibrillar collagen (FIB COL). GFP-βPix was immunoprecipitated from cell lysates under each condition to search for matrix-specific associated proteins. Coomassie blue staining of protein bound to βPix revealed a unique ~130 kDa band (<srGAP1) and a ~65 kDa band (<PPP2R1A) that mass spectrometry identified as srGAP1 and PP2A regulatory subunit A α isoform. "C" denotes bands from non-specific collagen binding. (**b**) HFFs were cultured overnight in 3D collagen gels, incubated with inhibitory integrin antibodies, (β_1-mAb 13, α_5-mAb 16, or α_2-P1E6) and allowed to migrate for a further 12-16 hours. Inhibition of β_1 or α_2, but not α_5, inhibited cell migration and spreading in 3D collagen. Experiment was performed independently at least twice with identical observations. (**c**) GFP-βPix isolated from knockdown/rescue fibroblasts migrating on fibronectin or fibrillar collagen was analyzed for candidate phosphopeptides that were unique to each ECM. The resulting phosphopeptides are displayed in tabular form, showing the peptide sequence with modified residue in lowercase letters, MASCOT ion score, specific modifications, and delta PPM of each peptide spectra. The two unique phospho-threonine peptides isolated while on fibronectin are outlined in red. (**d**) Quantification of cell elliptical factor 3D collagen of βPix knockdown/rescue cells expressing wild-type βPix and the phosphorylation variants. n = 24, 20, 23, and 19 cells for βPix sh#2, KDR-WT, T526E, and T526A were assessed across three independent experiments (mean ± s.e.m., one-way ANOVA with Bonferroni multiple comparisons correction). (**e**) Max projections of phalloidin-stained MDA-MB-231 knockdown/rescue cells expressing wild-type βPix or the βPix phosphorylation variants migrating in 3D collagen. Scale bars, 50 μm. (**f**) Quantification of morphology of MDA-MB-231 knockdown/rescue cells expressing wild-type βPix and the phosphorylation variants migrating in 3D collagen. Elongated cells defined as having an elliptical factor > 1.5. n = 34, 36, and 38 cells for WT, T526E, and T526A were assessed across three independent experiments. (**g**) Quantification of migration velocities of MDA-MB-231 knockdown/rescue cells expressing wild-type βPix or the phosphorylation variants migrating in 3D collagen. n = 23, 21, and 25 cells for WT, T526E, and T526A were assessed across three independent experiments (mean ± s.e.m., one-way ANOVA with Bonferroni correction). (**h**) Immunoprecipitation of GFP-βPix from βPix knockdown/rescue MDA-MB-231 migrating on fibronectin (FN) versus fibrillar collagen (FIB COL) additionally shows collagen-specific associations between βPix and PPP2R1A/srGAP1. Blot representative of three independent experiments. Statistical source data can be found in Supplementary Table 2, *** $P < 0.001$.

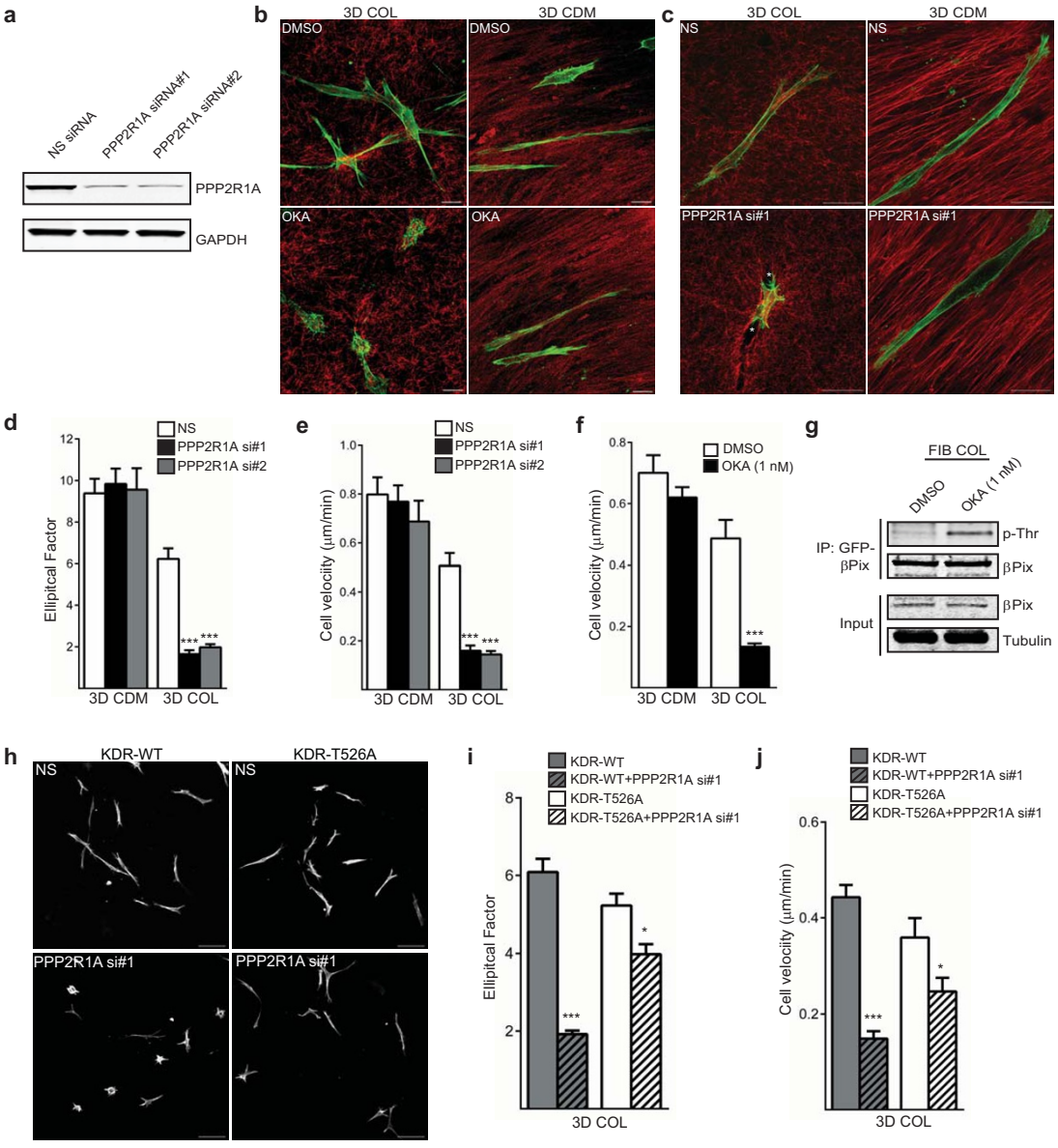

Supplementary Figure 5 (**a**) Single siRNA knockdown of PPP2R1A with two independent sequences. (**b**) Maximum projection of phalloidin-stained (green) HFFs in 3D collagen (red, reflection) or 3D cell-derived matrix (red, reflection) treated with DMSO or with the PP2A inhibitor okadaic acid (1 nM) overnight prior to fixation. Inhibition of PP2A resulted in collagen-specific morphological defects. Scale bars 25 μm. (**c**) Maximum projection of phalloidin-stained (green) HFFs in 3D collagen (red, reflection) or 3D cell-derived matrix (red, fibronectin immunostaining) treated with NS or with PPP2R1A siRNA #1. Scale bars 25 μm. (**d**) Quantification of morphology of PPP2R1A siRNA-treated HFFs in 3D collagen. n = 19-32 cells for NS, PPP2R1A si#1, PPP2R1A si#2 (both CDM and COL) were assessed across three independent experiments (mean ± s.e.m., one-way ANOVA with Bonferroni correction). (**e**) Quantification of migration velocities of PPP2R1A siRNA-treated HFFs in 3D collagen. n = 16-22 cells for NS, PPP2R1A si#1, PPP2R1A si#2 (both CDM and COL) were assessed across three independent experiments (mean ± s.e.m., one-way ANOVA with Bonferroni correction). (**f**) Quantification of migration velocities of okadaic acid-treated (1 nM) HFFs in 3D collagen and 3D cell-derived matrix. n = 19, 20, 20, and 20 cells for DMSO CDM, OKA CDM, DMSO COL, and OKA COL were assessed across three independent experiments (mean ± s.e.m, *t*-tests). (**g**) GFP-βPix knockdown/rescue fibroblasts migrating on fibrillar collagen were treated with DMSO or the PP2A inhibitor okadaic acid (OKA, 1 nM). Inhibition of PP2A with okadaic acid increased phospho-threonine levels on βPix during migration on collagen. Representative of at least three independent experiments. (**h**) Maximum projection of phalloidin-stained KDR-WT or KDR-T526A HFFs treated with NS or PPP2R1A siRNA #1 migrating in 3D collagen. Scale bars, 50 μm. (**i**) Morphological quantification of KDR-WT or KDR-T526A HFFs treated with NS or PPP2R1A siRNA #1 in 3D collagen. n = 40, 31, 35, and 38 cells for WT, WT+PPP2R1A si#1, T526A, and T526A+PPP2R1A si#1 were assessed across three independent experiments (mean ± s.e.m, *t*-tests). (**j**) Quantification of cell velocities in KDR-WT or KDR-T526A HFFs treated with NS or PPP2R1A siRNA #1 in 3D collagen. n = 26, 24, 24, and 24 cells for WT, WT+PPP2R1A si#1, T526A, and T526A+PPP2R1A si#1 were assessed across three independent experiments (mean ± s.e.m, *t*-tests). Statistical source data can be found in Supplementary Table 2, *** $P < 0.001$ * $P < 0.05$.

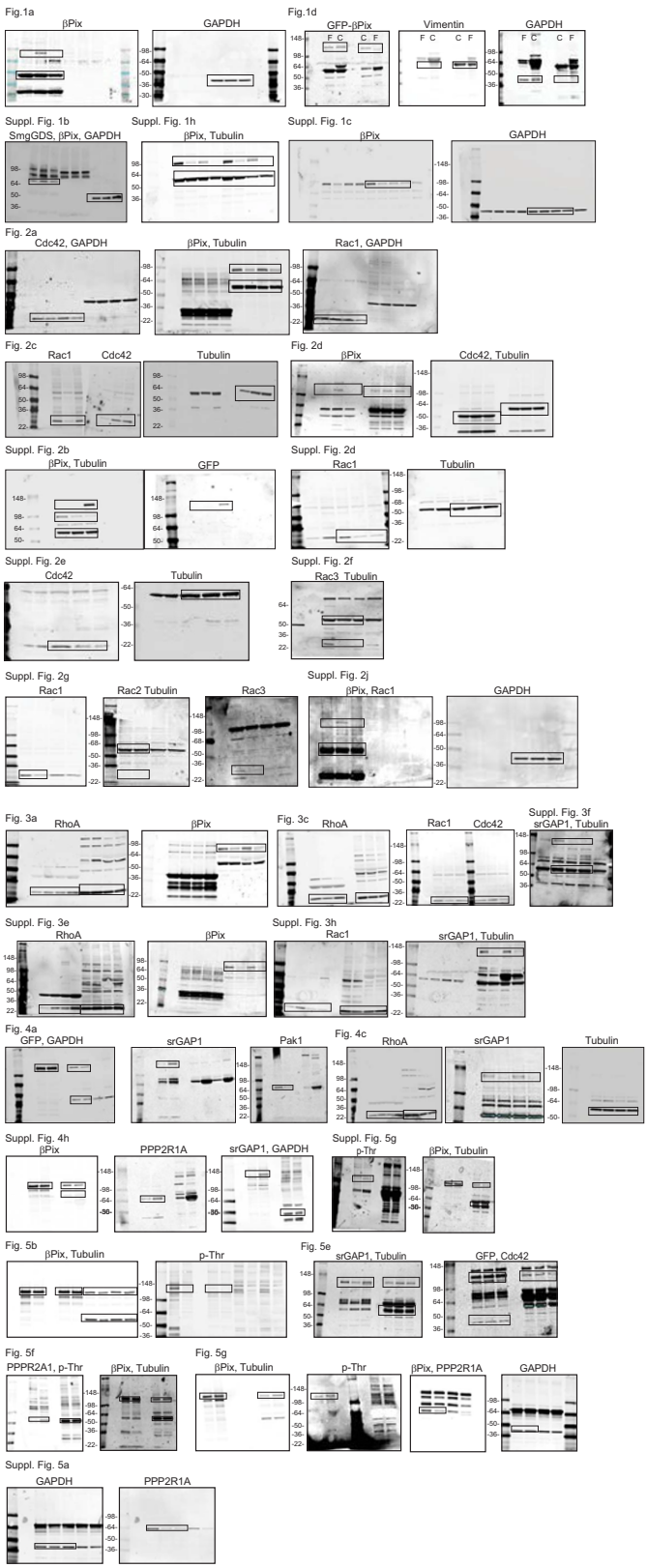

Supplementary Figure 6 Full scans of all blots that were presented in cropped form in figures in the primary and supplemental manuscript texts.

Supplementary Video Legends

Supplementary Video 1 Loss of βPix leads to severe, matrix-specific migratory defects in 3D collagen matrices. NS and βPix shRNA-expressing fibroblasts were allowed to spread in 3D collagen gels overnight and assayed for motility the following day. We find that βPix knockdown cells lack any form of persistent cell motility, and they are characterized by hyperactive spatially and temporally deregulated protrusions, rounded cell morphology, lack of defined leading and trailing edges, and elevated matrix contractility. Cells were allowed to migrate overnight in collagen and 24 hour timelapse was started the following morning, 5 minute frame rate, accelerated 5000x for display. Scale bar indicates 50 μm.

Supplementary Video 2 βPix is critical for migration in fibrillar collagen environments. Thin, fibrillar collagen substrates improved for optical imaging, but they retain the fibrillar structure of 3D collagen gels. We find that fibrillar collagen substrates are sufficient to recapitulate the βPix knockdown phenotype observed in 3D collagen, including the spatially and temporally deregulated protrusions, rounded morphology, lack of defined leading and trailing edges, and especially increased collagen contraction. Notably, the βPix knockdowns can be observed tearing holes in the fibrillar collagen matrix. Cells were allowed to migrate overnight in collagen and 24 hour timelapse was started the following morning, 5 minute frame rate, accelerated 5000x for display. Scale bars indicate 50 μm.

Supplementary Video 3 Cdc42, but not Rac1, phenocopies βPix knockdown in fibrillar collagen environments. Fibroblasts treated with NS, βPix, Cdc42, or Rac1 siRNA were plated on fibrillar collagen substrates and assayed for migration. Cdc42 knockdown effectively mimics βPix knockdown in fibrillar collagen environments, while Rac1 knockdown does not. Both βPix and Cdc42 knockdowns adhere to the surrounding collagen fibers and visibly tear physical holes in their adjacent regions. Cells were allowed to migrate overnight in collagen and 24 hour timelapse was started the following morning, 10 minute frame rate, accelerated 5000x for display. Scale bar indicates 50 μm.

Supplementary Video 4 Low-level overexpression of constitutively-active RhoA is sufficient to mimic βPix knockdown in fibrillar collagen environments. GFP-RhoAQ63L was transfected into HFFs, which were then plated on fibrillar collagen (FIB COL) substrate (center cell) or 3D collagen gels. Cells expressing low levels of GFP-RhoAQ63L as indicated by fluorescence intensity exhibited hyper-protrusive activity, increased collagen gel contraction (Supplementary Fig. 3c), and inability to migrate efficiently. Cells were allowed to migrate overnight in collagen and 24 hour timelapse was started the following morning, 10 minute frame rate, accelerated 5000x for display. Scale bars indicate 50 μm.

Supplementary Video 5 Knockdown of srGAP1 phenocopies the migratory defects of Cdc42 or βPix knockdown in 3D collagen. HFFs were treated with NS or srGAP1 siRNA and allowed to spread overnight in 3D collagen gels. Migration assays revealed hyper-protrusive activity, increased collagen gel contraction (Fig. 4d and evident in movie), and an inability to migrate efficiently. Cells were allowed to migrate overnight in collagen and 24 hour timelapse was started the following morning; 5 minute frame rate, accelerated 5000x for display. Scale bar indicates 50 μm.

Supplementary Table Legends

Supplementary Table 1 RNAi sequence information.

Supplementary Table 2 Statistics source data.